UNIVERSITÀ DEGLI STUDI DI PADOVA

DIPARTIMENTO DI INGEGNERIA CIVILE, EDILE E AMBIENTALE Department of Civil, Environmental and Architectural Engineering

MASER DEGREE IN ENVIRONMENTAL ENGINEERING

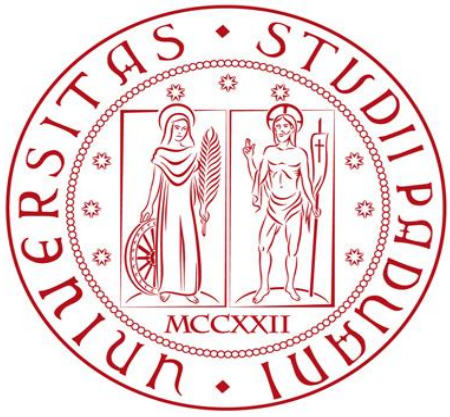

MASTER THESIS

3D GEOMECHANICAL ANALYSIS OF LAND DISPLACEMENTS DUE TO AQUIFER OVER-EXPLOITATION IN THE GEDIZ RIVER BASIN,TURKEY

Supervisor: **Prof. Teatini Pietro**

Co-supervisor: **Claudia Zoccarato**

Graduate Student: **Mahammad Aliyev**

1216004

Academic Year 2022/2023

Table of content

Abstract

The alluvial aquifer system of Gediz River basin, western Turkey, has been largely over-exploited during the last decades mainly for crop production. The lowering of the piezometric levels following groundwater pumping has caused significant land subsidence, up to a few centimeters per year. The thesis work is aimed at using the GEPS3D simulator, which is a three-dimensional geomechanical model developed at Dept. ICEA of Padova University, to simulate the displacement fields in the study area over the last 8 years. The factor forcing the aquifer deformation is represented by the pressure evolution has reconstructed in Dokuz Eylul University, Turkey, using MODFLOW. The results revealed that the highest land subsidence which was obtained in the range of 4 m. During the whole simulation period land subsidence reduced to 3.2 m. The study also evaluated the horizontal displacement and change of displacement components over time due to pressure fluctuation.

Chapter 1: Introduction

The Turkish economy heavily relies on the agricultural sector, and this trend is projected to persist in the coming years (Yercan, 2009). The demand for water in Turkey is rapidly growing due to the fast-growing economy and expanding industrial areas. Agricultural lands continue to be the largest water users in the country, with all agricultural lands being irrigated, mainly through surface irrigation (Van Loon, 2007).

The Gediz River Basin, located along the Aegean coast of Turkey, is a typical case where water scarcity and overexploitation of water resources for agriculture need to be addressed for sustainable management of its resources. The basin's extensive water resources systems are under pressure due to rapid industrial development, population growth, and related increases in agricultural production. Additionally, excessive groundwater withdrawal for agricultural purposes in the Gediz River Basin has led to significant declines in groundwater levels and subsequent land subsidence, which can have negative impacts on infrastructure, buildings, and the environment (Nilgun 2007).

Land subsidence is a global phenomenon that has occurred in numerous regions across the world due to different reasons such as excessive groundwater withdrawal, oil and gas extraction, mining activities, and natural geological processes. In recent years, the impact of land subsidence on infrastructure, buildings, and the environment has become increasingly apparent. For example in the San Joaquin Valley in California has been caused by groundwater pumping, groundwater-level declines, and land-use changes, leading to a decrease in flow capacity of water-conveyance systems and affecting irrigation water delivery. Multiple methods were used to measure vertical land-surface changes between 2007-2014, including InSAR, CGPS, and extensometer data.

The El Nido area had the highest InSAR-measured rate of 270 mm/yr, while the Pixley area had a rate of 90 mm/yr. Groundwater pumping increased during drought periods, causing historical lows in groundwater levels (Sneed 2015).Similarly inTianjin, China, has been experiencing land subsidence for 50 years due to excessive groundwater pumping. The subsidence has affected nearly 8,000 km2 of land, with a maximum cumulative subsidence of 3.22 m recorded in 2008. The highest subsidence rate was observed in the 1980s, reaching 110 mm/year, coinciding with a peak groundwater extraction of 1,200 million m3(Yi Lixin 2011). In Bangkok land subsidence has also been caused by excessive pumping of groundwater through deep wells, exacerbating the impact of subsidence on flood risk and foundation engineering. The subsidence rate peaked in the early 1980s at 120 mm/year and has since decreased, but the problem continues to worsen due to urban growth .The subsidence correlates with piezometric drawdown, with approximately 0.10 m3 of ground loss occurring at the surface for every 1 m3 of groundwater pumped. However, land subsidence will likely continue due to the time-dependent consolidation behavior of the soft clay layer and clay aquitards (Phien-wej 2005)

Dokuz Eylul University conducted an analysis of the Gediz River Basin (GRB) and developed a regional, three-dimensional transient groundwater flow model for the alluvial aquifer using the public-domain GUI ModelMuse. The modeling study aimed to simulate changes in groundwater storage related to land subsidence, improve previous basin-scale groundwater flow models, develop a mathematical model to advance understanding of the alluvial aquifer, and determine critical areas of decline in groundwater levels. The analysis provided critical information about the change in

groundwater levels over the past 8 years and showed that the Alaşehir-Sarıgöl aquifer is under significant water stress with an average depletion of 83.9 Mm^3 of groundwater storage per year (Alper et al., 2022).

The flow simulation accurately represents the regional patterns of groundwater flow in the GRB alluvial aquifer, yielding meaningful water balances consistent with previous estimation studies. To simulate land displacement in the Gediz River Basin, a three-dimensional finite-element geomechanical model was utilized, using the Geomechanical Elasto-Plastic 3D Simulator (GEPS3D) developed by the University of Padova (add a couple of proper references). The evolution of the piezometric head in time and space and the storage coefficient of the aquifer system, which forces and controls, respectively, the deformation of the system, was obtained from the results of the ModelMuse provided by Dokuz Eylul University. Also the geometry of the aquifer system was derived directly from the database used by Dokuz Eylul University.

The thesis is composed of the following several sections. The first chapter is focused in the explanation of mechanism of land subsidence and fundamental subsidence principle. Then, the area of study is described showing its climate, geology, land use and aquifer system. The next part of work describes the outcome of GRB groundwater flow model provided by Dokkuz Eylul University. The source and method of calibration are described properly. Finally, the application of the GEPS3D geomechanical simulator to the case study is described in detail. The model set-up is presented and the main outcomes, in terms of vertical and horizontal land displacements

cause by the variation of the pressure head over the period from 2013 to 2021 are simulated and properly described.

Chapter 2: Land subsidence due to aquifer overexploitation

2.1 Mechanisms of land subsidence due to aquifer overexploitation

The terms "groundwater overpumping" and "aquifer overexploitation" are increasingly being used in water-resources management due to climate change and rapid population growth, which are putting groundwater aquifers under pressure. This is particularly true in densely populated areas in arid and semiarid environments, making frequent monitoring of groundwater levels essential to identify areas experiencing rapid depletion of groundwater resources. To ensure sustainable water management of aquifers, especially in arid areas prone to drought, it is crucial to address these issues (Custodio, 2001; Rafiei, 2022; Gambolati 2021). When a pumping well starts withdrawing groundwater from an aquifer system, it causes a disturbance that spreads through the geological medium in space and time. A cone of depression forms around the well, causing a drop in fluid head that varies in intensity depending on various factors such as distance from the well, basin configuration, and hydro-geomechanical properties of the fluid and formation.

Compressibility is a crucial factor in determining medium deformation, as the decline in fluid piezometric head results in a decrease in pore pressure, leading to a transfer of stress from the fluid to the solid phase. This increases the effective stress in both the pumped units and adjacent formations, cause progressive drainage and compaction. The amount of compaction is primarily related to the compressibility of the compacting layers, and the resulting cumulative compaction of subsurface layers can cause the ground surface to subside (Gambolati and Teatini, 2015). The decrease in pore water pressure results in an increase in effective stress, which is borne by the grain-to-

grain contacts of the geological material. The increase in effective stress develops in both the pumped units and the adjacent formations (such as aquitards and confining beds) that compact, and the amount of compaction is primarily related to the compressibility of the compacting layers. The resulting cumulative compaction of subsurface layers can cause the ground surface to subside (Figure 2-1). Pore-water pressure can also increase when water is added to an aquifer through natural recharge or injection, which may partially reverse or mitigate subsidence in some settings (Gambolati 2021).

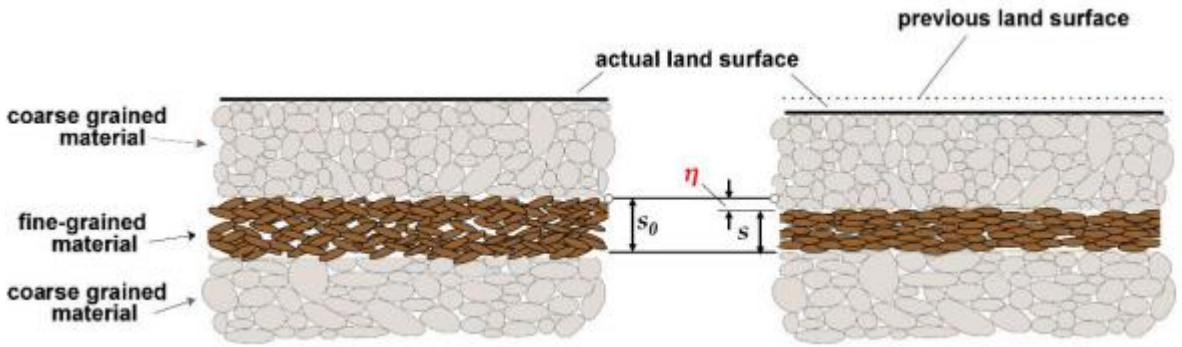

Figure 2- 1: Soil compaction occurs when there is a reduction in the amount of space between soil grains, while the grains themselves remain essentially unchanged in size

The principles of soil mechanics form the basis for theories on land subsidence. These theories consider soil as a collection of grains that are in contact with each other. For the purpose of analysis, the soil is assumed to be fully saturated with a degree of saturation equal to 1. To study the soil structure, a horizontal cross-section can be made through the soil, which intersects the contact points between the grains (Figure 2-2).

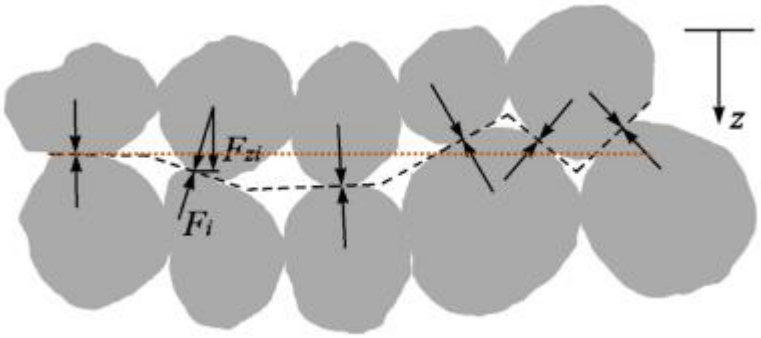

Figure 2- 2: Porous medium vertical cross section

The geostatic stress, denoted by σ_c, refers to the weight of a column of soil exerting pressure on a unit horizontal area at a particular depth. This weight is a combination of the solids and fluids present in the pores. According to Terzaghi's equation (1923, 1925), it reads:

$$\sigma_c = \sigma_z + p$$

The geostatic stress, also known as the "total vertical stress", it the sum of the effective integranular stress σ_c, which is the actual stress that grains exchange at the contact points, and the fluid pressure p. In the case of a pumped confined aquifer, where the pores drain slowly, the geostatic stress remains constant during pumping. However, the pore pressure decreases leading to an equal increase in the effective intergranular stress, σ_z. This increase in effective stress causes the formation being pumped to compact.

Figure 2-3 illustrates the qualitative behavior of the void ratio (e) versus the effective intergranular stress. As the effective intergranular stress increases, the formation compacts and the void ratio decreases. As a simplifying assumption, we assume that the grains are incompressible, meaning that they are much stiffer than the

porous matrix, especially in shallow soils. This implies that the compaction of the porous medium is primarily due to the reduction of pore volume, resulting in a decrease in both the void ratio and the porosity (ϕ).

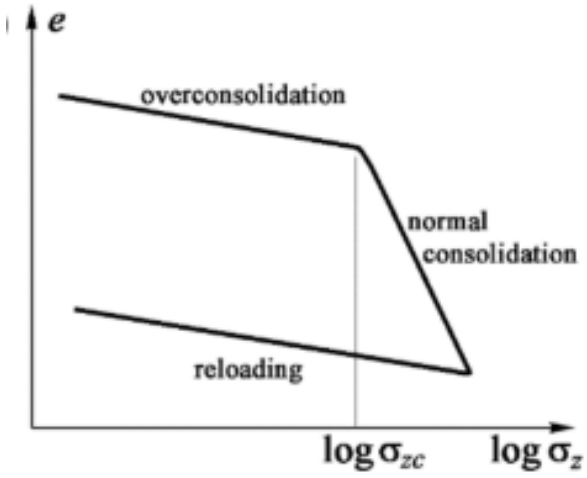

Figure 2- 3: Over-consolidation refers to a soil that has experienced a maximum effective stress equal to σzc in the past, which was subsequently reduced.

2.2 Equilibrium equations

There are two main approaches to analyzing and modeling deformation in aquifer systems, which are based on the relationships between head, stress, compressibility, and groundwater flow. One approach follows conventional groundwater flow theory, as developed by Jacob, while the other is based on linear poroelasticity theory, as proposed by Biot (1941). Both approaches are rooted in the principle of Effective Stress, as formulated by Terzaghi (1923, 1925). Assuming that solid grains are incompressible, the Terzaghi principle in a 3D setting can be written n terms of stress tensors (Galloway 2011):

$$\sigma'_{ij} = \sigma_{ij} + \delta_{ij} p$$

with *i* and *j* the coordinate axes, σ'_{ij} the tensor of the total stress, σ_{ij} the tensor of the effective stress and $\delta_{ij}$the Kronecker delta. The deformation of a porous body is solely caused by variations in the effective stress, following the Cauchy equations of equilibrium. When considering changes from an initial undisturbed state of equilibrium, these equations are expressed using incremental effective stress and pore pressure, as shown in Equation below:

$$\frac{\partial \sigma_{xx}}{\partial x} + \frac{\partial \tau_{xy}}{\partial y} + \frac{\partial \tau_{xz}}{\partial z} = \frac{\partial p}{\partial x}$$

$$\frac{\partial \tau_{yx}}{\partial x} + \frac{\partial \sigma_{yy}}{\partial y} + \frac{\partial \tau_{yz}}{\partial z} = \frac{\partial p}{\partial y}$$

$$\frac{\partial \tau_{zx}}{\partial x} + \frac{\partial \tau_{zy}}{\partial y} + \frac{\partial \sigma_{zz}}{\partial z} = \frac{\partial p}{\partial z}$$

The symbols σ_{xx}, σ_{yy}, and σ_{zz} denote the incremental normal effective stresses along the x, y, and z coordinates, respectively, while the terms $\partial\sigma_{xx}$, $\partial\sigma_{yy}$, and $\partial\sigma_{zz}$ refer to the incremental shear stresses. Stresses σ and deformations ε are linked through constitutive relationships. In the case of a linear elastic and isotropic soil, the Hooke law is used:

$$\sigma_{ij} = \lambda\varepsilon_{\alpha\alpha} + 2\mu\varepsilon_{ij}$$

$$\sigma_{xx} = \lambda\varepsilon_{\alpha\alpha} + 2\mu\varepsilon_{xx}$$

$$\sigma_{yy} = \lambda\varepsilon_{\alpha\alpha} + 2\mu\varepsilon_{yy}$$

$$\sigma_{zz} = \lambda\varepsilon_{\alpha\alpha} + 2\mu\varepsilon_{zz}$$

$$\sigma_{zz} = \lambda\varepsilon_{\alpha\alpha} + 2\mu\varepsilon_{zz}$$

$$\sigma_{xy} = 2\mu\varepsilon_{xy}$$

$$\sigma_{yz} = 2\mu\varepsilon_{yz}$$

$$\sigma_{xz} = 2\mu\varepsilon_{xz}$$

where:λ, μ are Lame constants, $\varepsilon_{\alpha\alpha} = \varepsilon_{xx} + \varepsilon_{yy} + \varepsilon_{zz}$ is the volumetric strains.

Therefore, for an isotopic porous medium, the geomechanical properties can be fully characterized using the two independent parameters, i.e. the Lame' constant λ and the shear modulus μ. These two parameters are related to the most widely known Young modulus E and Poisson's ratio ν through the relations:

$$\lambda = \frac{\nu E}{(1-2\nu)(1+\nu)}$$

$$\mu = \frac{E}{2(1+\nu)}$$

Finally, notice that oedometric soil compressibility c_b is related to E and ν as follows:

$$c_b = \frac{(1+v)(1-2v)}{(1-v)E}$$

If Hooke's low is substituted into the Cauchy equations, we can derive the equilibrium equations for a porous medium subjected to pore pressure variations p within it, expressed in terms of displacements. For an isotropic medium, these equations can be written as:

$$G\nabla^2 u + (\lambda + \mu)\frac{\partial \varepsilon}{\partial x} = \frac{\partial p}{\partial x}$$

$$G\nabla^2 v + (\lambda + \mu)\frac{\partial \varepsilon}{\partial y} = \frac{\partial p}{\partial y}$$

$$G\nabla^2 w + (\lambda + \mu)\frac{\partial \varepsilon}{\partial z} = \frac{\partial p}{\partial z}$$

The system of equations applies to an isotropic medium, and there are three equations with four unknowns: u, v, w, and p. Therefore, the groundwater flow equation must be added to the system (Gambolati, 2021)

2.3 Modeling land subsidence

Modelling land subsidence requires a detailed understanding of the geological and hydrogeological properties of the area of interest. Advanced technologies such as 2-D and 3-D seismic surveys, airborne-electromagnetic investigations, well-logs, and exploration boreholes can provide valuable information on the subsurface geology and hydrogeology. In addition, monitoring techniques such as Global Navigation Satellite Systems (GNSS) and Interferometric Synthetic Aperture Radar (InSAR) can accurately measure ground surface movements from space. To accurately measure shallow and deep aquifer system compaction, single-level cable and multi-level magnetic borehole extensometers can be used. (Gambolati, 2021)

Anthropogenic land subsidence modeling and forecasting tools have been continuously improved with the advancements in computer hardware and measurement technology. These tools can help in determining and distinguishing among multiple causes of land subsidence and can be effectively combined with measurement techniques. Once the models have been calibrated to the observed history of the aquifer, they can be used to evaluate various future scenarios of groundwater use and develop integrated resource management programs that take into account environmental and socio-economic impacts. The models are particularly useful in evaluating the adverse consequences of fluid extraction in the medium to long term, especially for urban flood management of coastal areas and in other cases of environmental vulnerability. They are designed to operate on even the most advanced parallel computer architectures, enabling them to handle complex heterogeneous geologies and geometries. One simulator is

GEPS3D (Geomechanical Elasto-Plastic 3-D Simulator) code, which was developed at the University of Padova. GEPS3D has been used in various regional-scale geomechanical applications and utilizes an advanced block FSAIILU preconditioner to solve large linear systems arising from the finite element implementation on parallel supercomputers. (Gambolati and Teatini, 2015)

Chapter 3: Characteristics of study area

3.1 Gediz River Basin

The Gediz River Basin is one of the most water-stressed basins, which is located in the western part of Turkey, with a drainage area of 17034 km^2. The length of the river is about 400 km and is flows from east to west directly to the Aegean sea (Figure3-1). The river originates from various major springs that are located in Mount Murat in the northeast of the basin and Mount Bozdağ at an elevation of 2159 m Alper et al., 2022).

The groundwater bodies in the GRB are divided into three hydrogeological classes. The first class includes sedimentary units with extensive groundwater, formed mainly by alluvial deposits, and are known as the alluvial aquifer of the GRB. These units are concentrated in the Gediz graben area and contribute significantly to the total groundwater potential in the basin. The second hydrogeological class consists of consolidated units with local groundwater, and the third class comprises consolidated units with limited groundwater (DSI, 2014).

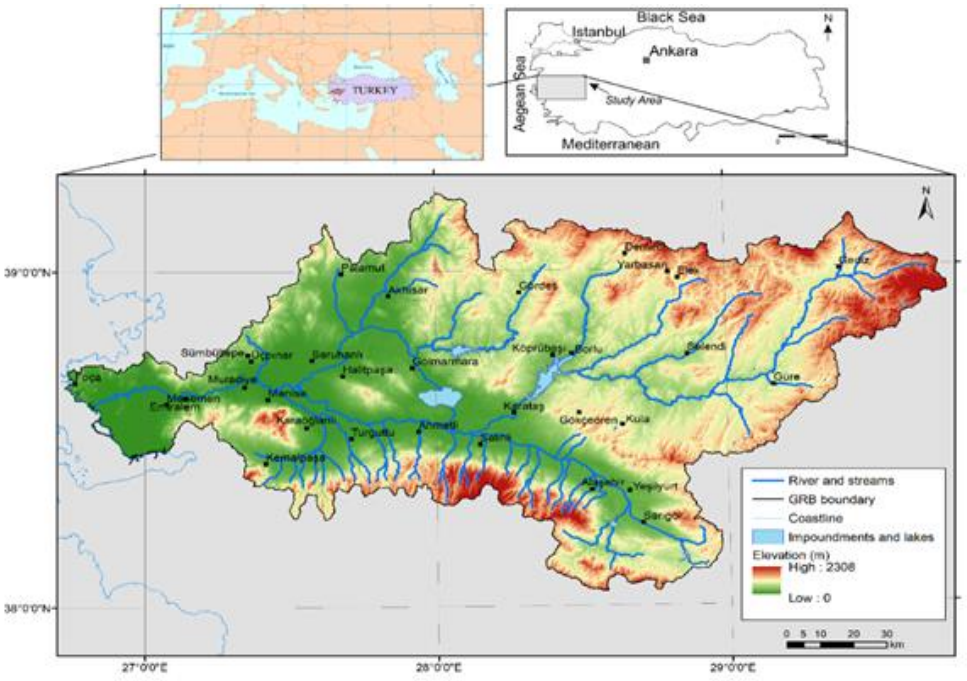

Figure 3- 1: Map and elevationof the Gediz River Basin

The study site selected for the RESERVOIR project is located in the alluvial aquifer of the Gediz River Basin, which is abundant in groundwater. The alluvial aquifer is mostly developed in the WNW-ESE directional Gediz graben, also known as the Alaşehir Graben, which follows the course of the Gediz River and the Alaşehir Creek, a tributary of the Gediz River Alper et al., 2022).

The total drainage area of Alaşehir sub-basin is 2710.5 km2 and the sub-basin has a very wide area. The altitude of the sub-basin, which is a typical depression basin, ranges from 83 to 2155 m from the sea level. The upper parts of the basin are surrounded by Bozdağ and Seyran mountains. The agricultural areas primarily rely on the shallow alluvial aquifer, which is formed from the alluvial deposits of the Alasehir Stream, for irrigation water (Baba, 2016).

3.2 Climate

The GRB region experiences a Mediterranean climate, which includes dry and hot summers and rainy and cold winters. The average temperature throughout the year is 15.2°C, and the mean annual precipitation is 617 mm, although this amount can vary depending on the location in the basin, ranging from 440 to 672 mm. Typically, the wettest months are January and February, while the driest are July and August. The average relative humidity in the basin is around 64%. In the modeling study, two meteorological stations within the study area were used to obtain climate data, one located in the north and the other in the south of the Alasheir Sarigol alluvial plain. The yearly long-term average precipitation for these stations are 526 mm and 665 mm. On a monthly basis, the wettest month is December, with a long-term average of 144.2 mm, while the driest month is August, with an average of 0.1 mm. The lowest average temperature (7.8 °C) occurs in January, while the highest average temperature (27.1 °C) occurs in July Alper et al., 2022).

3.3 Geology

The model domain extends over the Alasehir Graben. The structural pattern of the Gediz Graben is arc-shaped, measures 140 km in length, and 10-15 km in width (Sozbilir, 2022). Figure 3-2 provides the structural formation of the study area. The graben has been filled by Miocene to Recent sedimentary deposits that formed on the metamorphic rocks of the Menderes Massif. The geological sequence, listed from bottom to top, consists of Paleozoic gneiss, schists, and marble associations, followed by Neogene terrestrial sediments and Quaternary deposits. The evolution of the Menderes Massif is commonly explained by the core complex model, in which the

footwall comprises high-grade metamorphic rocks, such as gneiss, schist, and marble, and the hanging wall is composed of Miocene to Quaternary units with syntectonic Miocene-aged granites. The Neogene associations primarily consist of sandstone, conglomerate, claystone, limestone, and volcanic intercalations (Demirkesen 2019). Neogene and Quaternary sedimentary layers, primarily consisting of sandstone, conglomerate, claystone, limestone, and volcanic layers, overlay the basement rocks with an unconformity. Unconsolidated Quaternary deposits cover these formations across the plain. The alluvial sediments in the study area comprise clay, clayey sands, and gravel, forming a layer that ranges from 20 to a maximum of 320 m Alper et al., 2022).

The composition of the aquifer is mainly heterogeneous due to varying sediment facies. Parts of the aquifer are sub-consolidated, consisting of fragments from the basement rocks, while other parts are unconsolidated, composed of granular grains such as sands and silt. The nature of the aquifer in the basin shows semi-confined to unconfined features in certain locations. The Neogene sediments in the basin are comprised of sandy clayey beddings with low permeability. The alluvial succession, where the primary aquifer is found, ranges from 120 to 250 m depth based on the deep wells drilled in the study area. The discharge rate of groundwater produced from these wells is between 5.0 to 30 l/s (Demirkesen, 2019). The direction of groundwater flow in the alluvial aquifer was determined to be from south to northwest through an analysis of the water table (Sözbilir, 2002).

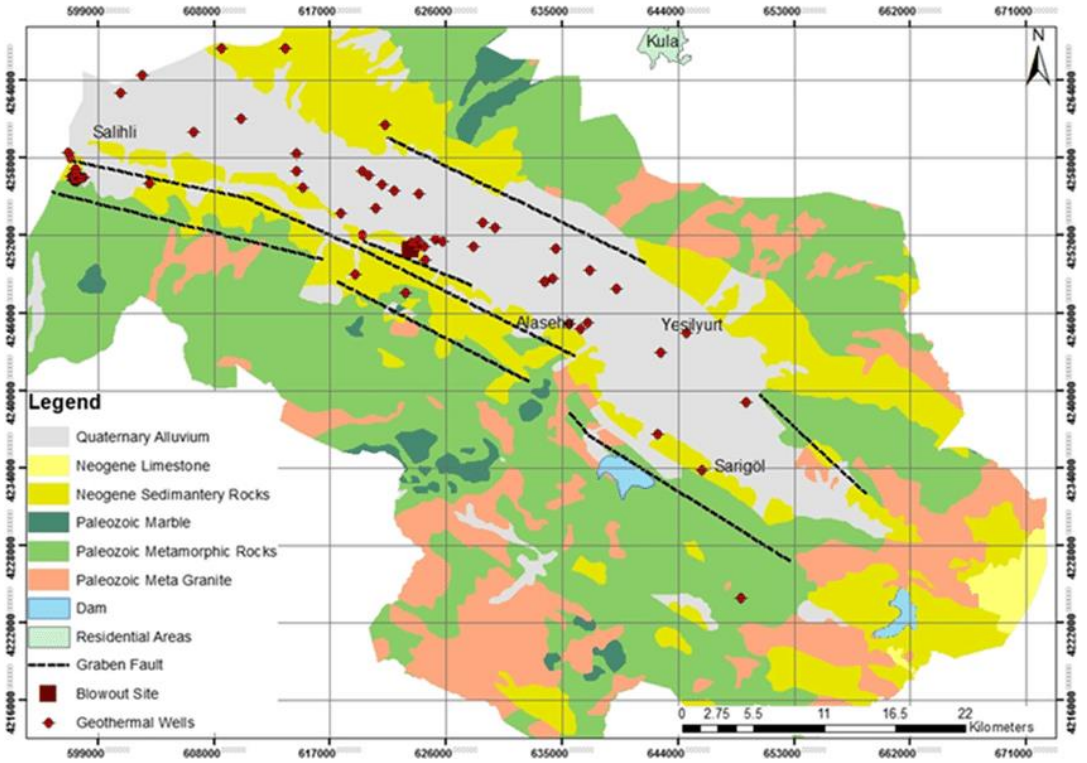

Figure 3- 2: Geological Map of the Alaşehir-Sarıgöl Plain, with simplified illustration of the different geological layers and structures (Demirkesen, 2019)

3.4 Landuse

The Gediz River Basin is home to approximately 1.34 million people living in towns and cities, while around 483 thousand people live in rural areas within the basin. The main economic activities in the region include agriculture, animal husbandry, food industry, textile industry, geothermal energy production, and mining. Various human activities, coupled with natural factors, have led to significant environmental challenges that have adversely affected the quantity and quality of groundwater resources in the basin. (Prima, 2019). The basin is primarily used for agriculture (Figure 3-3). The river network is managed by four main reservoirs, and four regulators are used for irrigation diversions. During heavy winter precipitation, river flows are stored in the primary

'Demirköprü' reservoir for release during the summer irrigation period. The crops grown within the basin include cotton, cereals, tobacco, and various fruits and vegetables such as grapes, olives, and melons (Yercan, 2004). Due to climatic conditions, irrigation is crucial for the success of agriculture, which is the main economic activity in the basin. As is common in many other agriculturally dominant basins, a significant portion of surface water resources (75%) is allocated to irrigation (Ucar, 2010).

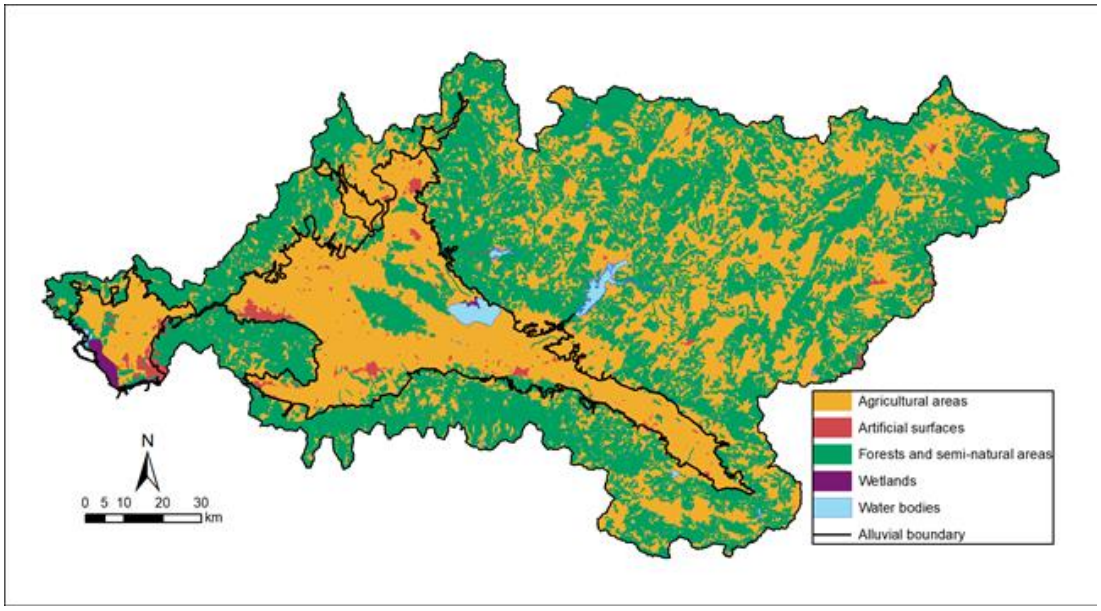

Figure 3- 3: Land use in the Gediz River Basin

The dominant land use in the Alaşehir-Sarıgöl study plain is agriculture, which covers 89.8% of the area. The primary crop in the area is vineyards, which covers approximately 73% of the cultivated surface; urban land use and industrial areas cover a small proportion of the study area, accounting for 4.1% and 0.7%, respectively Alper et al., 2022). The agricultural irrigation in the basin is mainly supplied by groundwater sources, as well as the Avşar Dam located in the western part of the basin and the

Derbent Dam located in the southern part of the basin (Tonkul, 2019). The population in the study area is mainly concentrated in the towns of Alaşehir, Yeşilyurt, and Sarıgöl, with a total population of about 117,000 inhabitants, including those living in rural areas Alper et al., 2022).

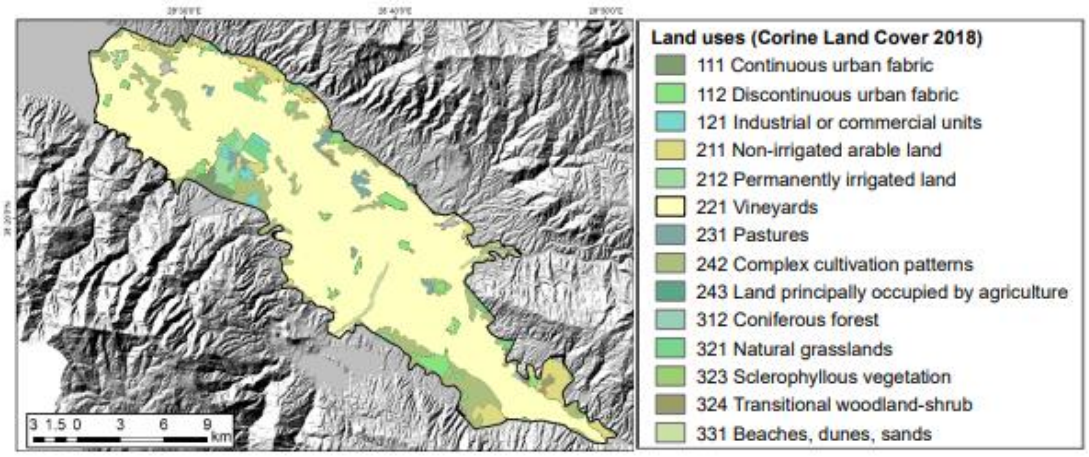

Figure 3-4: Map of Land Use Types in the Model Domain Area Using the CORINE-2018 Database Alper et al., 2022).

3.5 Aquifer System

The geological description of the study area suggests that the shallowest formations are Quaternary deposits, which are underlain by Neogene consolidated formations. The conceptual model developed for the study is bounded at the bottom by the bedrock formation below the Quaternary alluvial deposits, and borehole drilling logs were analyzed in detail to identify stratigraphic correlations. The stratigraphic data analysis indicates that the study area is controlled by graben faults and covered by alluvial material forming a thickness of up to 200 m. The combination of soft data from geophysical surveys with borehole log analysis resulted in stratigraphic column models from six borehole clusters (Figure 3-5). The area is characterized by five lithological units with alternating coarse-fine deposits. The uppermost layer is conceptualized as

permeable with silty sand materials, forming an unconfined aquifer, followed by a confining layer composed of clays and sandy clay materials. The aquifer layer below is again a permeable layer with predominantly sands and gravel, followed by another confining layer consisting of sandy clay. The deepest unit is a clayey-gravel layer underlain by a Neogene series bedrock. Permeable layers and clayey-gravel are the main aquifer systems of the study area, with most of the groundwater production wells drilled in the third layer. The geophysical surveying profiles indicate that high resistivity layers, such as sand and other coarse materials, alternate with lower resistivity layers, such as clay or sandy clay layers Alper et al., 2022).

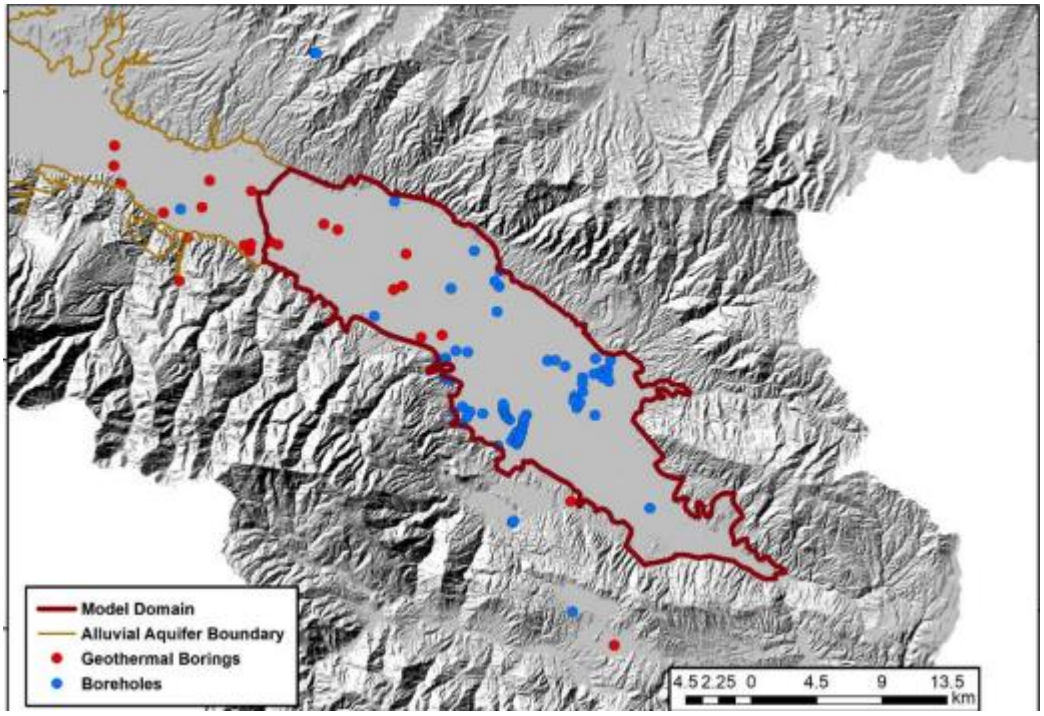

Figure 3- 5: Borehole locations to develop conceptual layers in GRB Alper et al., 2022).

3.6 Land Subsidence

Figure 3.6 shows the A-DInSAR map of deformation rates derived from Sentinel-1 processing with CPT algorithm. The measurements are in LOS with an angle of that varies from ~ 46.60 (West) to ~ 49.30 (East) from the normal to the Earth surface. The agricultural land cover surface is characterized by medium to high temporal decorrelation, so the coherence threshold was properly set to obtain a good compromise between spatial coverage and reliability. In contrast, the high relief areas on the basin borders with scarce vegetation show very good coherence and therefore very high spatial coverage. The ± 0.9 cm/year stability threshold is based on the standard deviation of the noise domain.

CPT results show surface terrain movement away (mainly land subsidence) and towards (mainly land upift) the LOS of the satellite, with peak LOS rates of -18.89 and 3.92 cm/year, respectively (Figure 3.6). The deformation shows very sharp edges. The maximum deformations away from the satellite (more than - 10 cm/year) are detected in the centre of the basin (agricultural land cover) and in the residential area of Yeşilyurt.

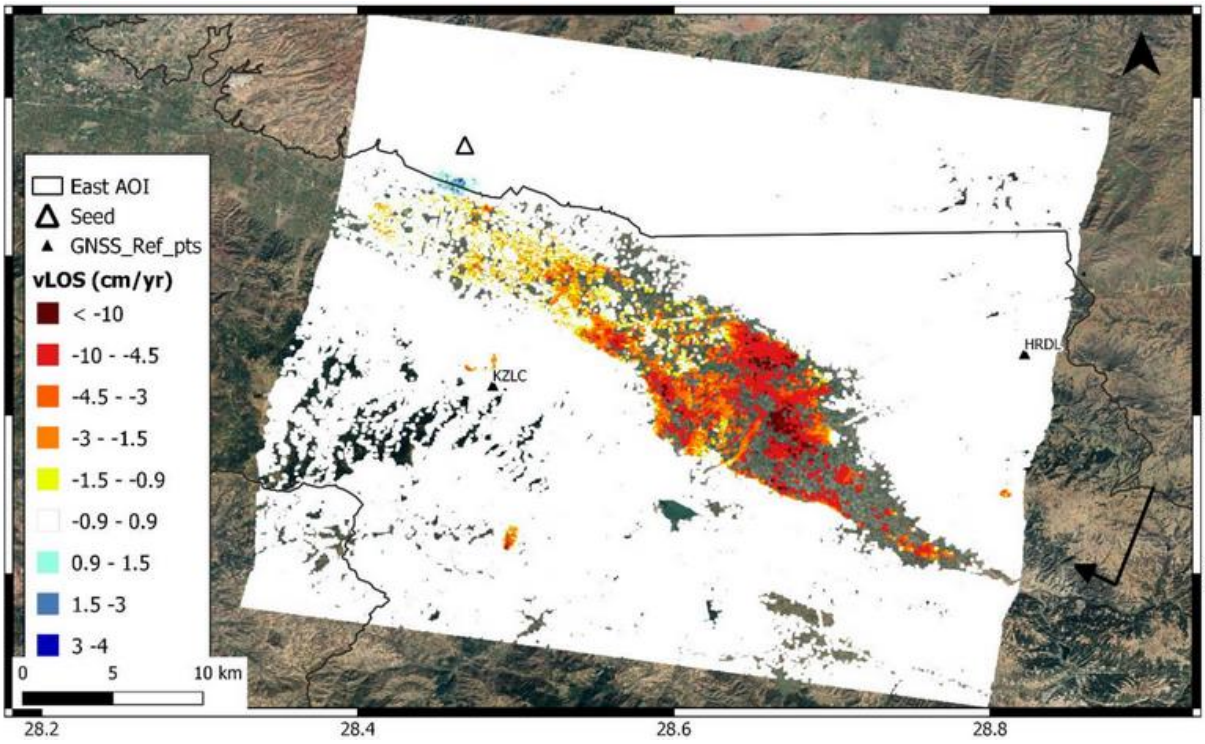

Figure 3-6: LOS velocity obtained by processing Sentinal-1 images using the CPT InSAR processing chain. Images cover the time frame from January 2019 to August 2021 (after Bru et al., 2021)

Chapter 4: GRB groundwater flow model

4.1 Model construction

The three-dimensional finite-difference groundwater flow model MODFLOW-2005 was utilized by the Dokuz Eylul University to simulate groundwater flow in the alluvial aquifer of the Gediz River Basin. ModelMuse is a graphical interface that supports various groundwater modeling programs. Recently, an update was made to enable ModelMuse to create input files for the parameter estimation software suite PEST when used with MODFLOW or SUTRA models (Winston, 2022).

To obtain a three-dimensional flow model using ModelMuse, its necessary to create a conceptual model of the aquifer system. The equation that governs the flow of fluid through a porous medium is typically obtained by applying the mass balance equation to the water that flows through an representative elementary volume (REV) of porous material:

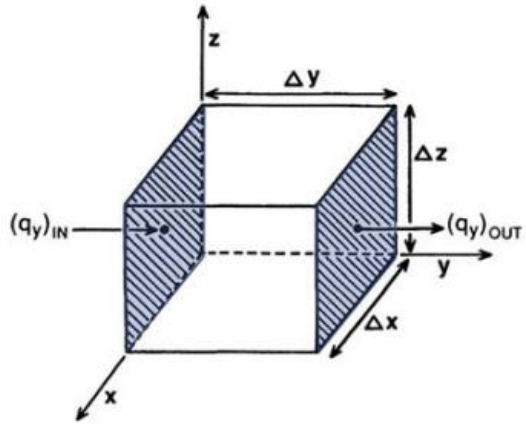

Figure 4- 1: The representative elementary volume (REV), which has dimensions of ($\Delta x \Delta y \Delta z$), illustrates the flow components in the direction of the y-coordinate axis.(Anderson, 2015)

$$Outflow - Inflow = \Delta \text{ storage}$$

where:

Outflow is the rate of water flowing out of the volume;

Inflow is the rate of water flowing into the volume;

Δstorage is the rate of change of the water stored within the volume.

Expressing the change in flow rate through the Representative Elementary Volume (REV) along the x-axis and z-axis by removing the IN and OUT subscripts and converting from a difference notation to a derivative.

$$\left(\frac{\partial q_x}{\partial x} + \frac{\partial q_y}{\partial y} + \frac{\partial q_z}{\partial z}\right) \Delta x \Delta y \Delta z = \Delta \text{ storage}$$

The statement explains that when analyzing fluid flow through a porous medium, it is important to consider the possibility of water sources or sinks within the REV. The volumetric inflow rate from these sources and sinks is denoted by W^* ΔxΔyΔz, where W^* is positive when water is being added to the system and negative when water is being removed from the system.

It is conventionally assumed that change in water storage ΔV is positive when there is a decrease in hydraulic head (Δh), meaning that water is being released from storage. The rate of in the mass water stored within the REV can be expressed as a function of the piezometric head change Δh:

$$\frac{\Delta \mathrm{V}}{\Delta \mathrm{t}} = -S_S \frac{\Delta \mathrm{h}}{\Delta \mathrm{t}} \Delta \mathrm{x} \Delta \mathrm{y} \Delta \mathrm{z}$$

the final form of the water balance equation:

$$\frac{\partial q_x}{\partial x} + \frac{\partial q_y}{\partial y} + \frac{\partial q_z}{\partial z} - W^* = -S_S \frac{\Delta \mathrm{h}}{\Delta \mathrm{t}}$$

The equation presented in the statement is not very practical in real-world applications because it is difficult to measure the specific discharge (q) directly. Darcy's Law (q=-K grad h) is a fundamental equation that relates specific discharge (q) to head (h), where the gradient of h (grad h) is a vector. The hydraulic conductivity tensor (**K**) plays an important role in this relationship. The specific discharge vector, q, has components that can be expressed in terms of the hydraulic conductivity tensor and the gradient of head as follows (Anderson, 2015):

$$q_x = -K_x \frac{\partial \mathrm{h}}{\partial \mathrm{x}};\ q_y = -K_y \frac{\partial \mathrm{h}}{\partial y};\ q_z = -K_z \frac{\partial \mathrm{h}}{\partial z}$$

Substituting, the governing equation that describes the three-dimensional movement of constant-density groundwater in saturated porous media reads.

$$\frac{\partial}{\partial \mathrm{x}}\left(K_{xx} \frac{\partial \mathrm{h}}{\partial \mathrm{x}}\right) + \frac{\partial}{\partial \mathrm{y}}\left(K_{yy} \frac{\partial \mathrm{h}}{\partial y}\right) + \frac{\partial}{\partial \mathrm{z}}\left(K_{zz} \frac{\partial \mathrm{h}}{\partial z}\right) = S_S \frac{\Delta \mathrm{h}}{\Delta \mathrm{t}} - W^*$$

The equation shown above describes the flow of water through a porous medium, such as an aquifer. The variables in the equation include hydraulic conductivity (Kxx, Kyy, Kzz), hydraulic head (h), volumetric flux (W), specific storage (Ss), and time (t). (Anderson, 2015) .

4.2 Spatial and Temporal discretization

The MODFLOW model grid was developed by the Dokuz University, Turkey (Alper, 2022). It consists of 5 layers, 242 columns, and 188 rows, covering a surface area of 319 km^2. The active cells in all 5 model layers are 73810.

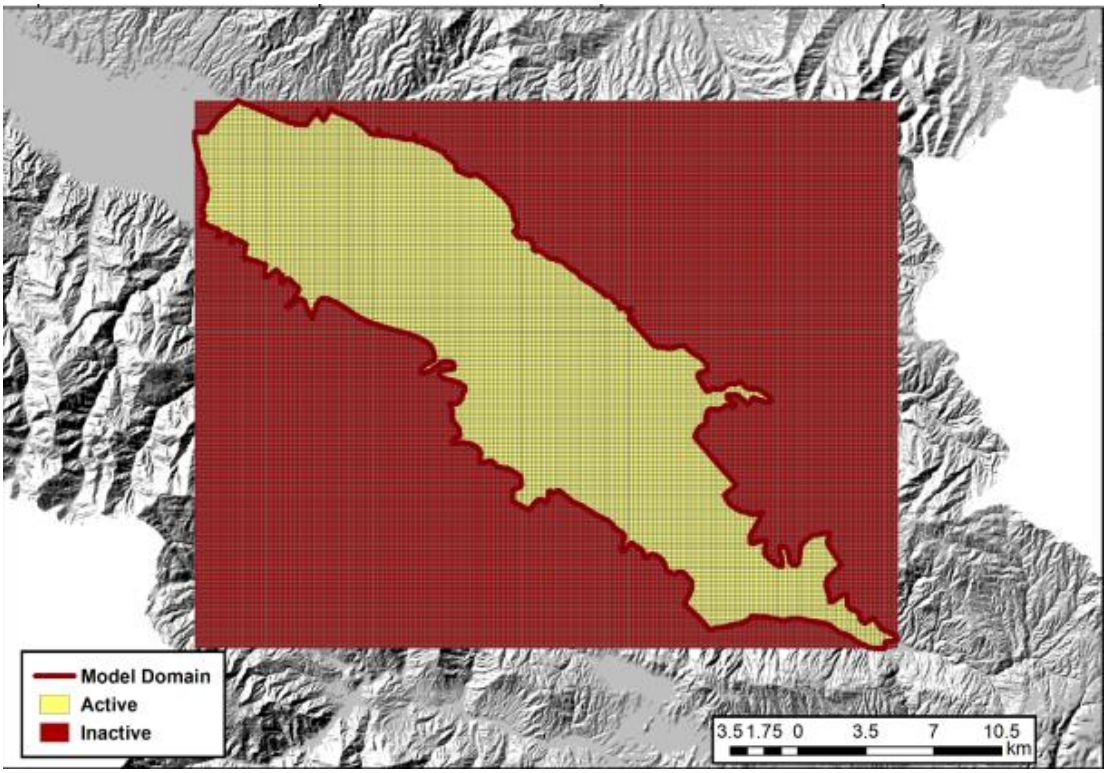

Figure 4- 2: Numerical study model grid of Alasehir-Aluvial plain (Alper et al., 2022).

Vertical discretization is an important step in groundwater flow modeling as it allows to reproduce more accurately flow and transport processes in multiple layers of the subsurface. In this study, the five model layers were based on the hydrogeological units delineated in the conceptual model, which likely reflect variations in lithology, hydraulic properties, and/or other factors that can affect groundwater flow (Figure 4-3). The top and bottom elevations of each layer were interpolated across the entire model

domain using data points from stratigraphic columns developed for the conceptual model. This allowed for the creation of a continuous three-dimensional grid of active cells with a uniform spatial resolution of 150 m by 150 m Alper et al., 2022). In this study, the stress periods were set to represent monthly conditions over a simulation period of 93 months, i.e. from October 2013 to June 2021. The selection of this simulation period was based on the time frame of the InSAR-derived land subsidence analysis period and the availability of meteorological data used to calculate groundwater recharge. The hydrologic stresses on the aquifer during the stress periods were caused of various factors, such as net groundwater recharge, groundwater withdrawal rates through pumping wells, surface water interaction with Alaşehir Creek, and head-dependent flows over the model boundaries. The use of constant time steps in the model, assigned in units of days, resulted in a total of 2830 days of simulation time, allowing for the evaluation of the temporal changes in the aquifer system over an extended period (Alper et al., 2022).

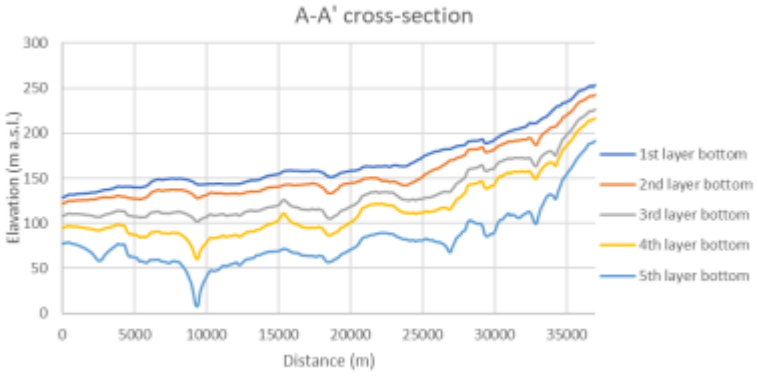

Figure 4- 3: Elevation of model layers in GRB (Alper et al., 2022).

4.1.3 Initial and boundary conditions

The initial head distribution of the flow model represents the hydraulic head specified for each grid cell at the start of the simulation period in October 2013. These initial head values were obtained by running a separate transient simulation of the same model for a warm-up period of 4 years. During this warm-up period, recursive hydrologic conditions of the first simulation year were implemented to obtain a stable hydraulic head distribution. The solution of the final time step of this warm-up simulation was then assigned as the initial head array for the transient flow model that simulates the period of interest. This approach ensures that the initial head distribution used in the simulation represents a realistic and stable condition that is consistent with the hydrologic conditions of the region. (Alper et al., 2022).

The use of the general-head boundary package GHB as a boundary condition for lateral groundwater flow is a common approach in groundwater modeling. By specifying a reference head far from the boundary, the GHB package allows for the simulation of external sources or sinks of groundwater. The use of hydraulic head distribution maps obtained from observation data ensures that the GHB head parameter values are representative of the true groundwater conditions. By dividing the boundary into polylines and assigning GHB boundaries to all layers, the model is able to accurately simulate the lateral groundwater flow into and out of the aquifer system. (Alper et al., 2022).

4.1.4 Hydraulic Parameters

Hydraulic conductivity and storage coefficient are important parameters to describe the movement of groundwater. Transmissivity data was estimated using an

empirical relationship and corresponding hydraulic conductivity values were calculated by dividing transmissivity by the well screen length . Specific capacity data from 249 wells was also used to inform the model (Figure 4-4). The initial horizontal hydraulic conductivity of certain layers in the model was assumed to be homogeneous with specific values. The vertical anisotropy ratio was also assumed to be 10. The model calculates the flow of groundwater between adjacent model layers based on the thickness and the vertical hydraulic conductivity of each layer (Alper et al., 2022).

The study used storage coefficients derived from pumping tests in 10 wells within the same study area. The aquifer storage coefficient in the study area ranged from 0.01 to 0.2, with an average of 0.07. In some areas, the coefficient was less than 0.01, indicating a semi-confined aquifer (Figure 4-5) However, two wells in the Neogene units had storage coefficients ranging from 0.018 to 0.067 (Tongul, 2019).

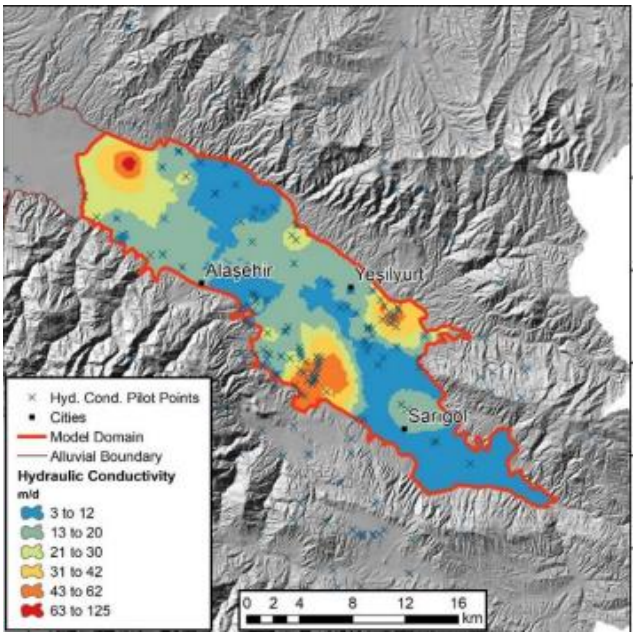

Figure 4- 4: Spatial distribution of hydraulic conductivity used in the groundwater flow model for the alluvial aquifer in the Gediz River Basin. (Alper et al., 2022).

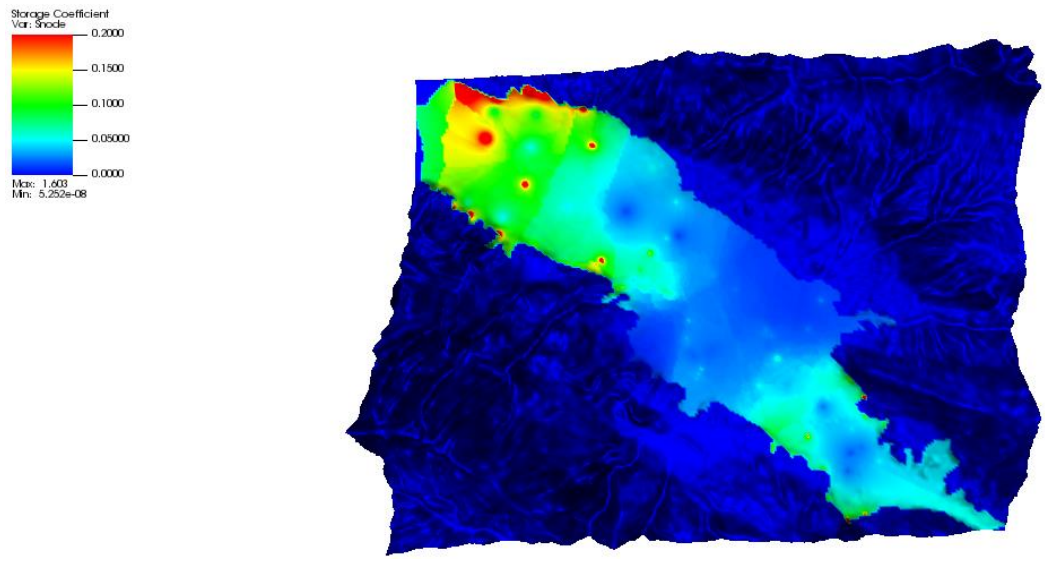

Figure 4- 5: Initial storage coefficient distribution in the GRB alluvial aquifer flow model

4.2 Source and sinks

4.2.1 Groundwater recharge

Estimating groundwater recharge is an important aspect of hydrogeologic studies, and it is typically achieved through methods such as multiplying water-level fluctuations by specific yield or applying water budget models and the water-balance method (Lee, 2006). The Recharge package (RCH) is used in in MODFLOW to simulate the influx of recharge water into the aquifer. The recharge rates were applied to the uppermost active grid cell in each vertical column of the model and varied over time for each stress period. Additionally, recharge rates were assigned as a spatially heterogeneous distribution, meaning they were distributed unevenly across the model domain Alper et al., 2022). The water balance is presented in the Figure 4-6 below, where groundwater fluxes act on control volume:

$$R = P + SW - ET - R$$

where P is the precipitation, SW change in soil water content, ET- evapotranspiration, R-runoff.

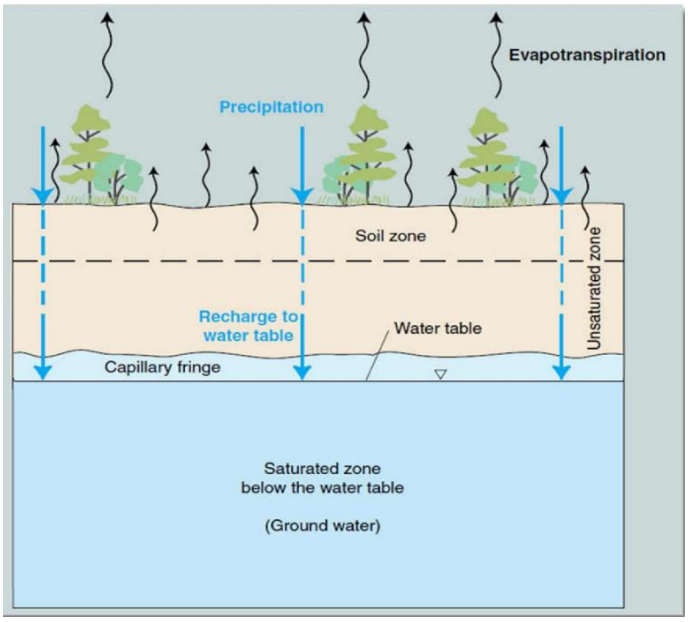

Figure 4- 6: Schematic diagram of the recharge to the water table (Day 2019).

Water balance models rely heavily on accurate measurement and computation of precipitation, which serves as the primary input. Therefore, the reliability of water balance computations largely depends on the accuracy of measuring and computing precipitation from a network of stations (Xu, CY. 1998). The study utilized precipitation data sourced from the General Directorate of Meteorology (MGM). The daily data sets were collected from meteorology stations located in Alaşehir and Sarıgöl, and monthly precipitation totals were derived from the daily data for a period of 8 years (2013-2018). The data was then spatially averaged using Thiessen polygons (Alper et al., 2022).

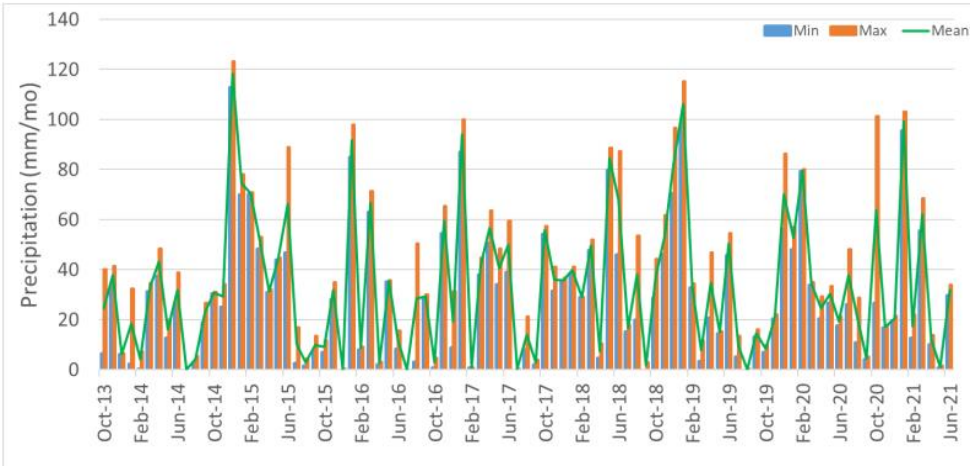

Figure 4- 7: Monthly precipitation data for the study area were collected and processed to obtain spatially-averaged values.

The Figure 4-7 indicates that there is a higher amount of precipitation during February each year compared to June, where there is relatively less precipitation. The process of estimating actual evapotranspiration (ETa) is crucial in the management of crops and water resources. ETa is made up of two sub-processes, evaporation from the surface and transpiration through plants, which are not easy to measure directly (Senay 2020). For the model actual evapotranspiration data (Figure 4-8) layers with a resolution of 500 meters were obtained specifically from the Terra Net Evapotranspiration databaseAlper et al., 2022).

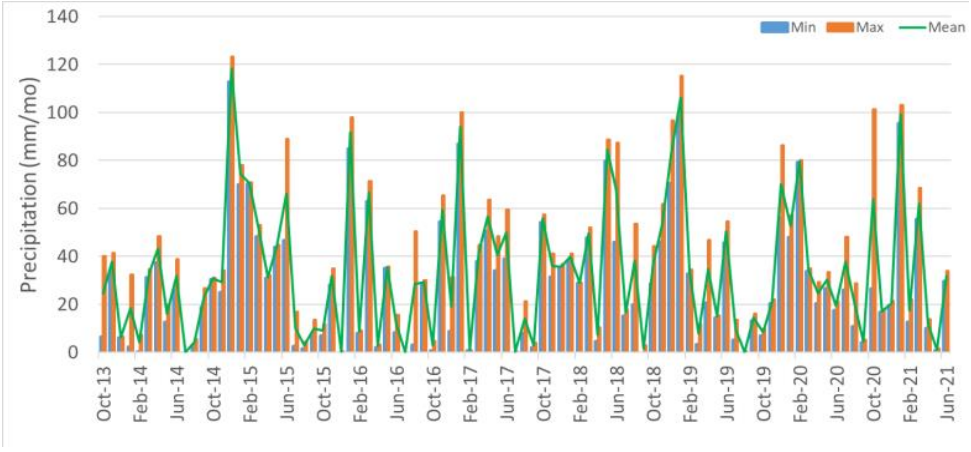

Figure 4-8: Graph provides the monthly actual evapotranspiration rates were obtained

Soil water content and runoff time were obtained from the ERA5-Land database. ERA5-Land is a database that offers a thorough description of water and energy cycles over land in a uniform and consistent manner over a specified production period (Sabater, 2019). The database contains four bands with a resolution of 11132-m for the volumetric soil water layer, representing the top four layers from the ground surface to a depth of 2.89 meters Alper et al., 2022). Surface runoff (Figure 4-9) refers to the portion of rainfall that enters a stream or other surface water body immediately after it falls. (Balasubramanian, 2017). Runoff rates are stored in a separate band. An ArcGIS script was created to automate the calculation of monthly changes in soil water content (Figure 4-10) using this data Alper et al., 2022).

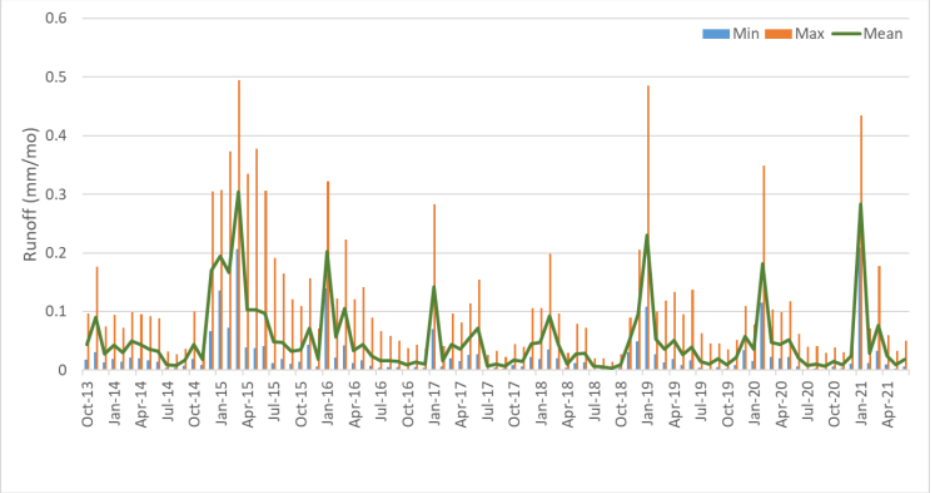

Figure 4- 9. Monthly time series of runoff data

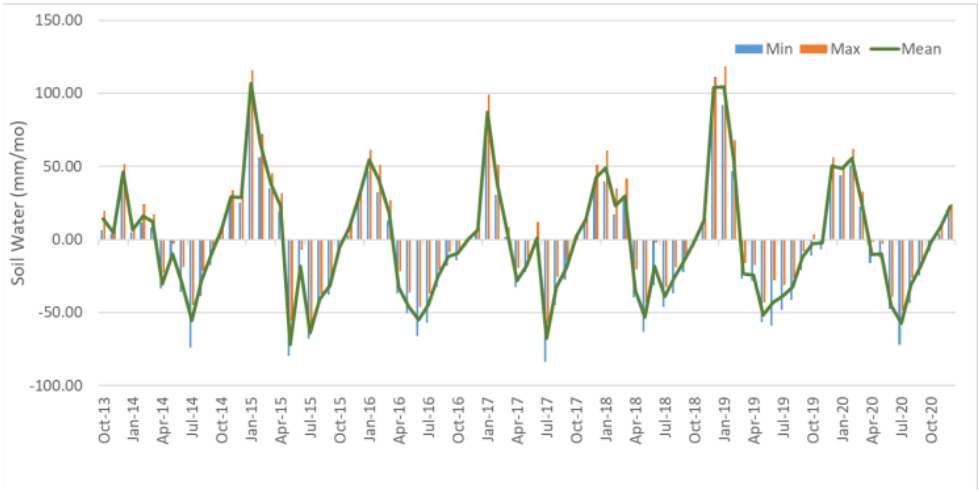

Figure 4- 10. The monthly changes in soil water content

4.2.2 Pumping wells

The model includes two types of pumping wells, irrigation wells and public water supply (PWS) wells (Figure 4-11), that withdraw groundwater from model layers 3 and 5. The locations of the PWS wells are based on actual data and are approximately accurate, while the locations of the irrigation wells are unknown and were estimated using fictitious wells distributed across areas used for crop irrigation. The model domain is dominated by vineyards, which make up 73% of the land area. The calibration head targets used in the model calibration process were obtained from reliable sources, including the 2nd Regional Directorate of the State Hydraulic Works and an independent study. The use of multiple sources helps to ensure the accuracy and reliability of the calibration dataset. A total of 22 wells were used for the calibration, and 395 observation records were screened for potential outliers to ensure the reliability of the data. (Alper et al., 2022).

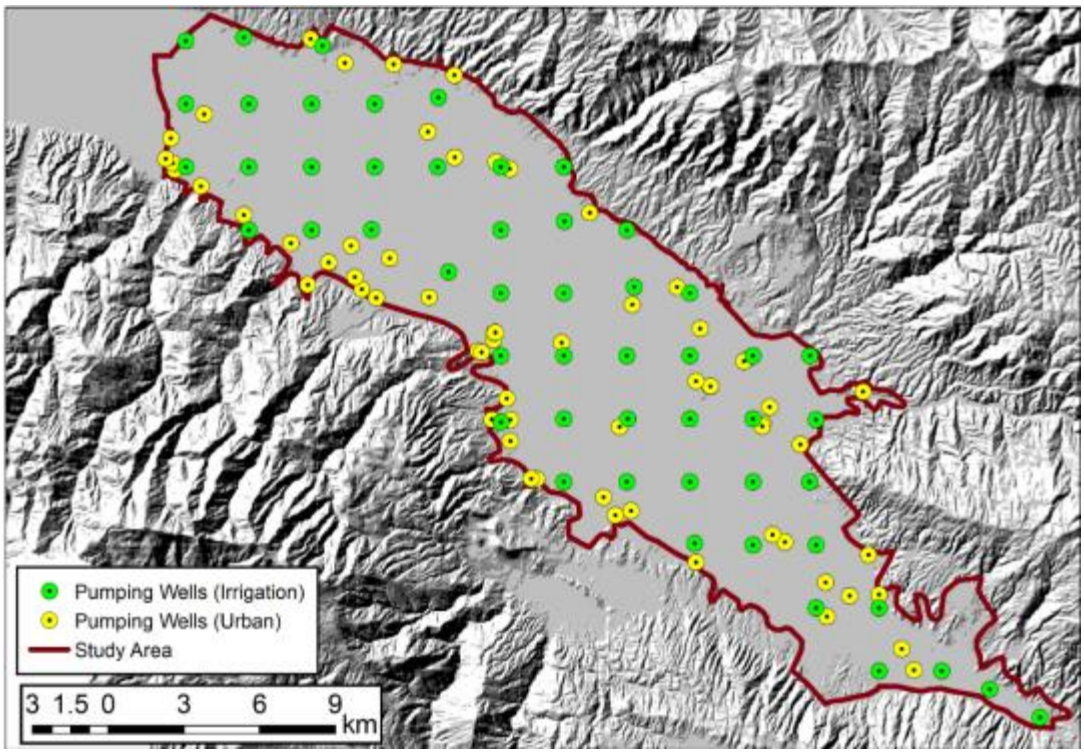

Figure 4- 11: The map illustrates locations of pumping wells in GRB

4.3 Calibration results

Figure 4-12 show the simulated potentiometric surface and groundwater flow directions during the dry and wet seasons, respectively, in the third aquifer. Groundwater flow is mostly from the southeast to the northwest, with depressed potentiometric surfaces observed around Sarıgöl and Yeşilyurt during the dry season. Groundwater levels are generally higher during the wet season, with minimum and maximum head values of 108 and 178 m, respectively. In some parts of the aquifer, groundwater level fluctuations are noticeable, while in other parts, the seasonal difference is less significant.

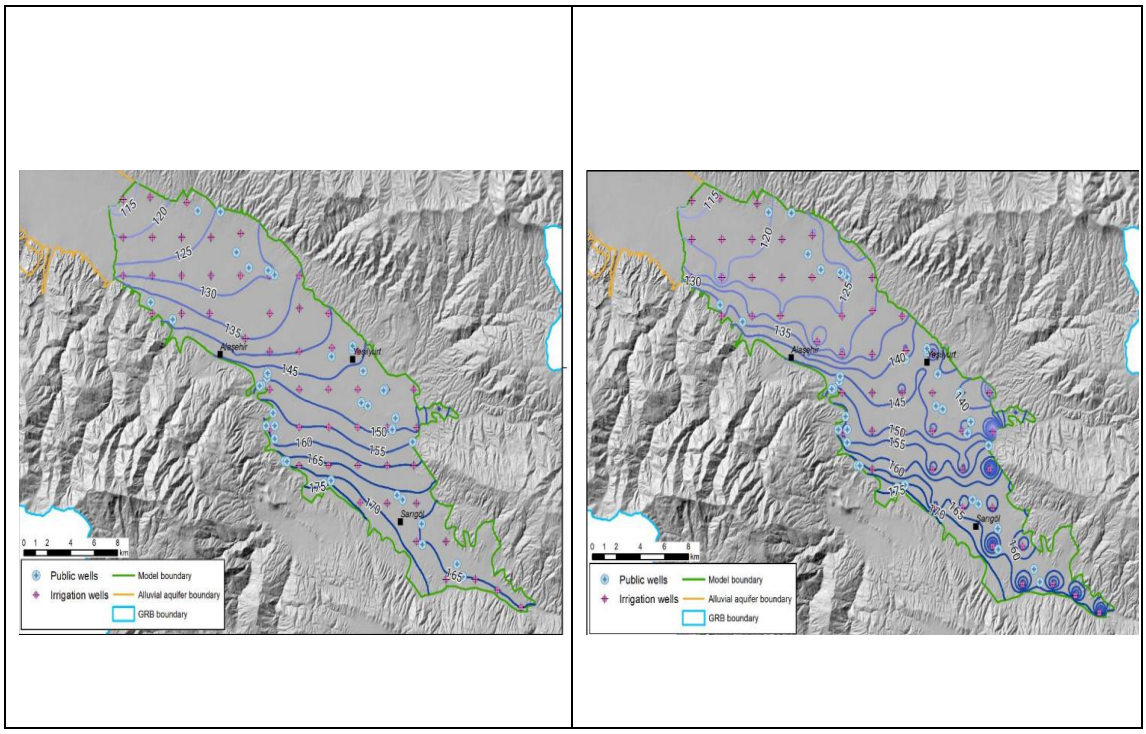

Figure 4- 12: The distribution of hydraulic head in the third layer of the groundwater flow model for the month of September, which was calculated using the model solutions during the simulation period. (Alper et al., 2022).

Figure 4-13 shows the simulated drawdown in the potentiometric surface for all 5 layers from September 2013 till the June 2021. The figure was analyzed to identify areas in the domain where groundwater exploitation is causing significant declines in the water table. The changes in groundwater levels cause a variation in the water volume stored in the aquifer system. According to the model results, at the end of the 8-year period, the groundwater levels in the east of Yeşilyurt and northeast of Sarıgöl had declined by up to 133.9 m. The model also indicates regions in the study area where water stored in the aquifer may have increased. These regions are visible along the southern boundary of the alluvial plain, and this could be explained by mountain-front recharge.

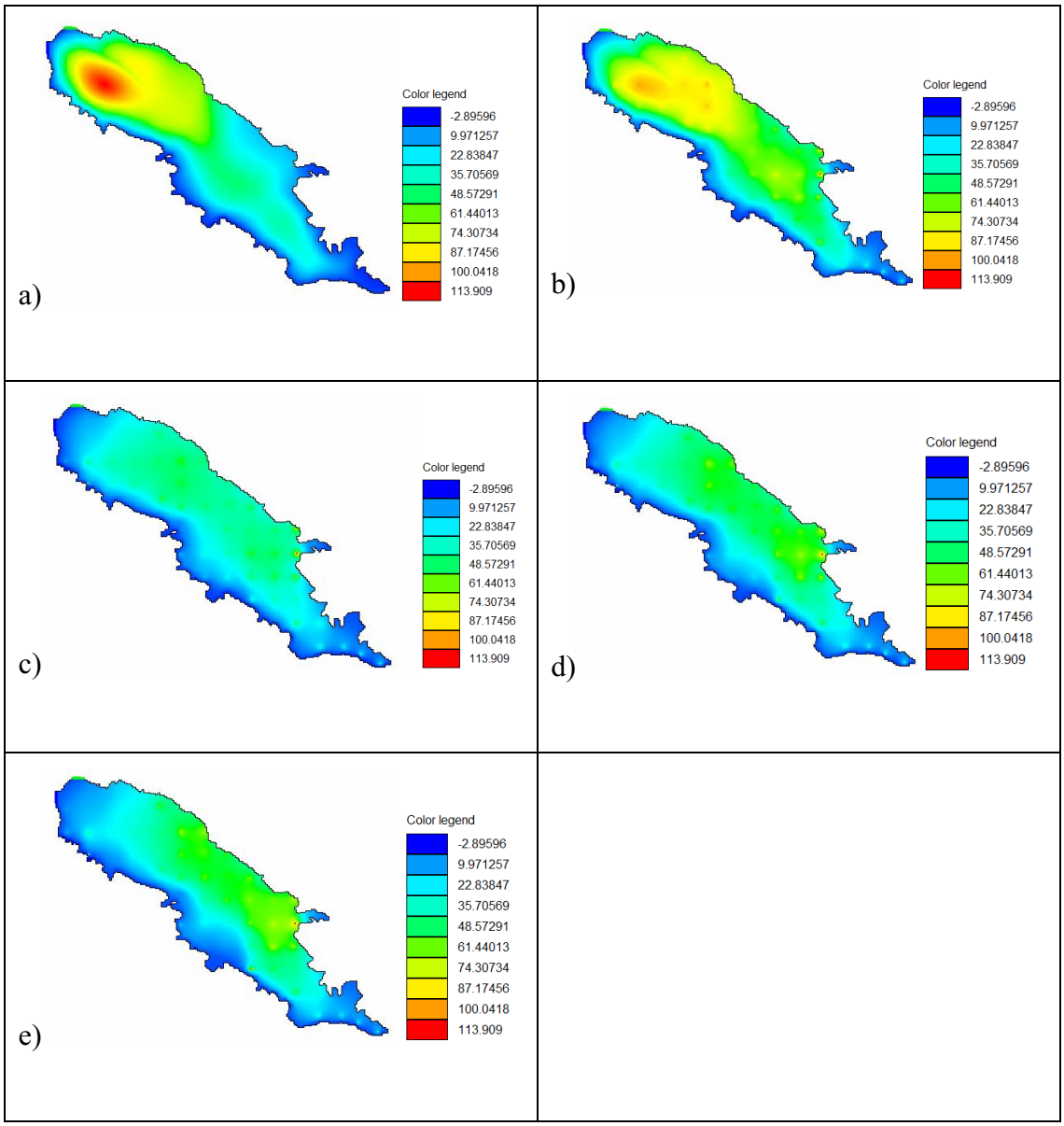

Figure 4-13. The results of the MODFLOW simulation in terms of groundwater drawdown that has occurred in all layers of the model since the start of the simulation. Each picture refers to one layer of the GRB: a) first layer, b) second layer, c) third layer, d) fourth layer and e) fifth layer

Chapter 5: Modeling 3D displacements in the River Gediz Basin

5.1Model setup

The 3D displacements caused by groundwater withdrawals in the Gediz River Basin was simulated using the GEPS3D, which is a three-dimensional geomechanical simulator developed at Dept. ICEA of Padova University. The modelling study was based on the set-up and outcomes of the ModelMuse model provided by the Dokuz Eylul University. Specifically, the results of the groundwater flow model, in terms of pressure change were used as input forcing factor in GEPS3D. Moreover, the consistency between the two models required the use of geomechanical parameters that agree with the storage coefficient calibrated with the groundwater flow simulations.

5.1.1 Spatial discretization in GEPS3D.

From the original data. which were mentioned before, the spatial discretization of the three-dimensional model grid which were provided in ModelsMuse consisted of 5 layers, 242 columns and 188 rows. ModelMuse, which is based on a finite difference (FD) method, provided the solution in terms of piezometric head change on each grid element. GEPS3D is a simulator based on a finite element (FE) approach and provides the solution (as displacements along the x, y, and z directions) on each node of mesh. To make the shift of the ModelMuse outcome into GEPS3D input as simple, straightforward and accurate as possible, a hexahedral finite element mesh was generated respecting perfectly the geometry of the ModelMuse grid, with the FE nodes located on the corners of the FD grid element. The FE mesh thus resulting is composed of 225’335 elements. Moreover, two FE layers were added at the model bottom with the same number of nodes/elements as in the shallower part derived directly by the ModelMuse grid. The reason of this step is properly explained in the next chapter. The

final mesh used for the geomechanical simulation by GEPS3D (Figure 5-1) consists of 315’469 elements and 318’472 nodes.

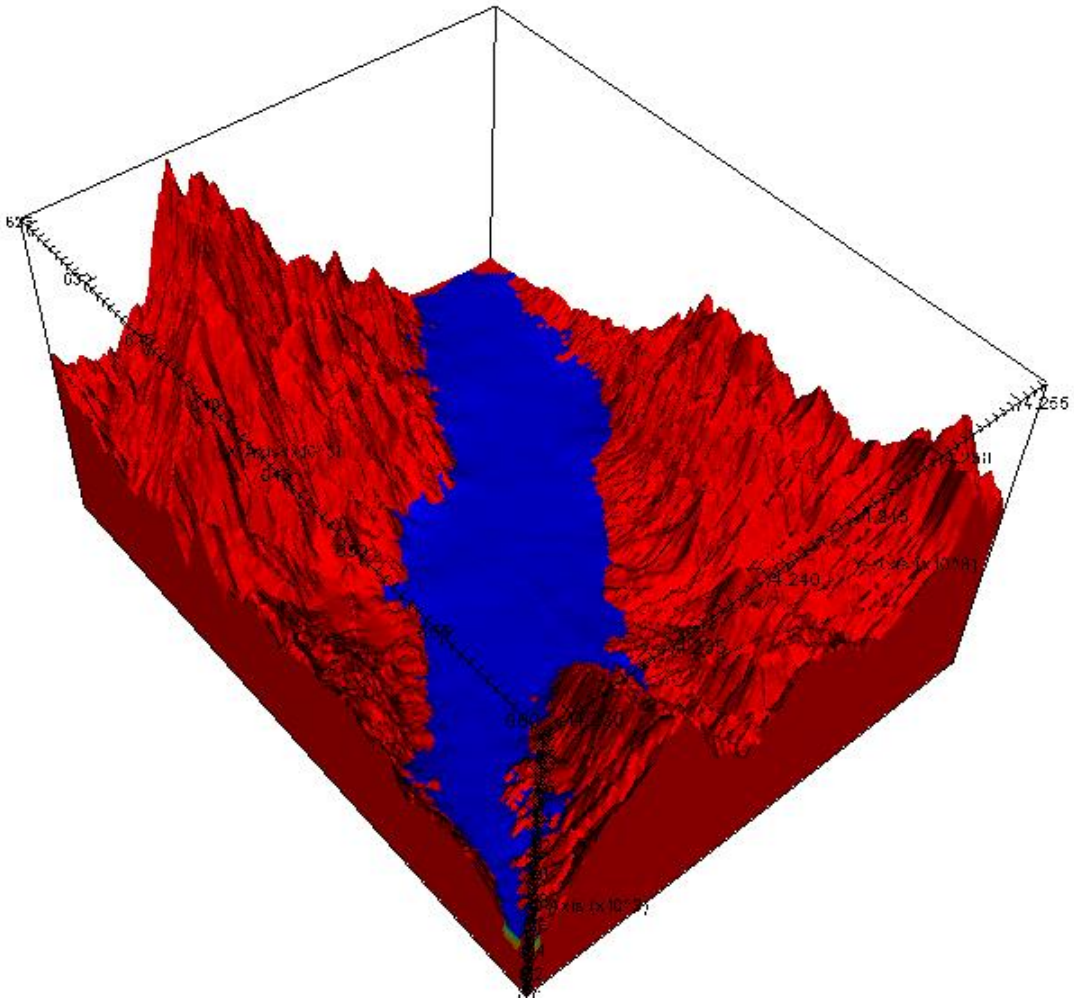

Figure 5- 2 The view of the GRB finite element model which was simulated by GEPS3D. The red color indicates mountains and the blue is the sedimentary valley of the study model. Only the “blue” cells were active in the ModelMuse simulations, i.e. no head evolution was computed in the rock part

5.1.2 Temporal discretization

How it was mentioned before in the description of ModelMuse analysis provided by Dokkuz Eylul University, the simulated time interval was divided in 93 time steps, covering the period from October 2013 to June 2021. The same time intervals were used in GEPS3D. The simulator solved the equilibrium equations and provided in output the West-East, South-North, and vertical displacements for 93 months (2830 days) covering the 8-year simulation period.

5.1.3 Boundary condition

Boundary conditions in a three-dimensional geomechanical model require to specify the displacement (or stress) vectors on the nodes located on the model boundaries. Generally, null displacements are prescribed on the bottom and lateral boundaries, while a free-stress condition is assigned to the model top (i.e., the nodes on the surface are free to move depending on the stressors developed within the model). Application of null displacements on the model bottom would significantly affect the model outcome if the model bottom corresponded to the bottom of the exploited aquifer system. To avoid this limit, two additional (FE) layers were added on the bottom of the groundwater model domain. Specifically, in this case, the additional layers will enable the implementation of a zero-displacement boundary condition at a distance from the geologic units undergoing pressure depletion, thus preventing the emergence of unphysical boundary effects on the model solution. The inclusion of the extra layers allows the zero-displacement boundary to be located far enough from the geologic units experiencing pressure depletion, minimizing the impact of boundary conditions on the model outputs. Figure 5-2 shows a vertical section of the model grid where the two

added layer are clearly visible. The same spatial discretization (150 m) of the shallower units was used in the added 2 layers.

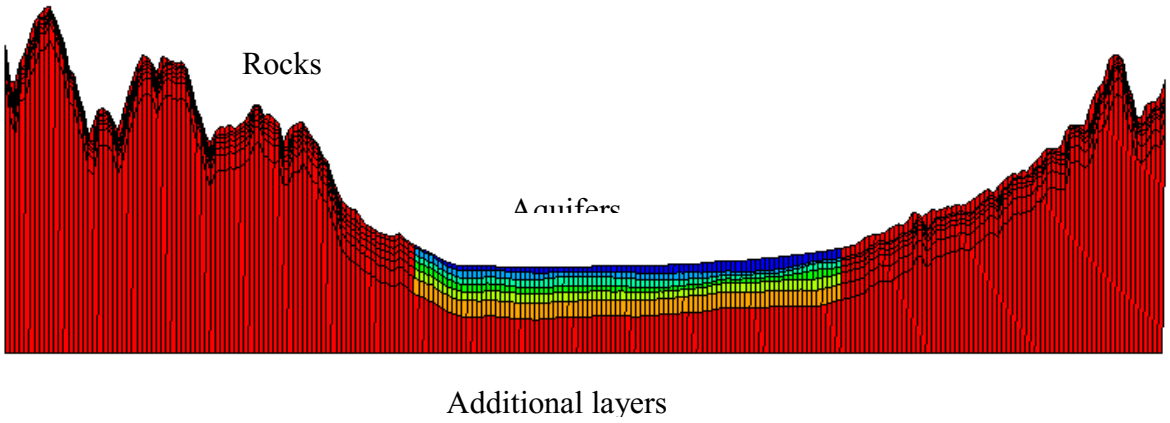

Figure 5- 3 Vertical section of the FE model showing the 2 additional layers added on the model bottom.

5.1.4 Geomechanical parameters

All the mesh elements are active in the geomechanical model. The model computes the displacement pattern also for the element representing the rocky ridges bounding the alluvial valley. Obviously, being much stiffer than sedimentary material and not interest by a pressure head variation, the displacement of the rock (red color in Figures 5-1 and 5-2) cells will be negligible.

The geomechanical parameters in GEPS3D, i.e. the Young modulus E and the Poisson ratio ν, for the rock has been assumed constant and equal to $15.07\ x\ 10^8$ and 0.25, respectively. For the elements corresponding to the sedimentary units, the Poisson ratio was assumed uniform and equal to 0.25. Concerning the Young modulus, the value varied from cell to cell and was computed from the elastic storage assigned in ModelMuse using the following relationships. The groundwater flow equation for an isotropic homogeneous porous medium can be written simply as

$$K\nabla^2 h = S_s \frac{\partial h}{\partial t}$$

where K is the hydraulic conductivity, h is the hydraulic head, t is time, and S_s [L^{-1}] is the specific storage. The specific storage coefficient is defined as:

$$S_s = \gamma(c_b + \phi\beta)$$

where c_b is the oedometric bulk compressibility, ϕ the medium porosity, and β the water volumetric compressibility.

For an isotopic porous medium, the geomechanical properties can be fully characterized using the two independent parameters E and ν:

$$c_b = \frac{(1+\upsilon)(1-2\upsilon)}{E(1-\upsilon)}$$

5.2 GEPS3D results: Seasonal evolution

The analysis focused on the evolution of the displacement field associated to the groundwater withdrawal from the aquifer system in the Gediz River Basin. Four times were selected within the time period spanned by the simulation to show the subsidence behavior. The results were reported for the driest period (September) and wettest period (April) of the year. Water extraction from the alluvial aquifer system is the highest during September to meet the demands of crop irrigation. As a result, the aquifer pressure may decrease more during this period, leading to larger land displacements. The GEPS3D outcomes were reported in September and April of the years 2015, 2017, 2019 and 2021. Figure 5-3 provides a map of the study model with the position of 5

nodes (from A to E) and with 2 vertical sections AA' and BB' where the model outcomes are shown. The nodes are located in various parts of the domain where different vertical and horizontal displacements were obtained. Specifically, node A is located in the Yesilyurt region, while nodes B, C, and D are located in the southern part of the GRB basin, and node E is situated in the northwestern region.

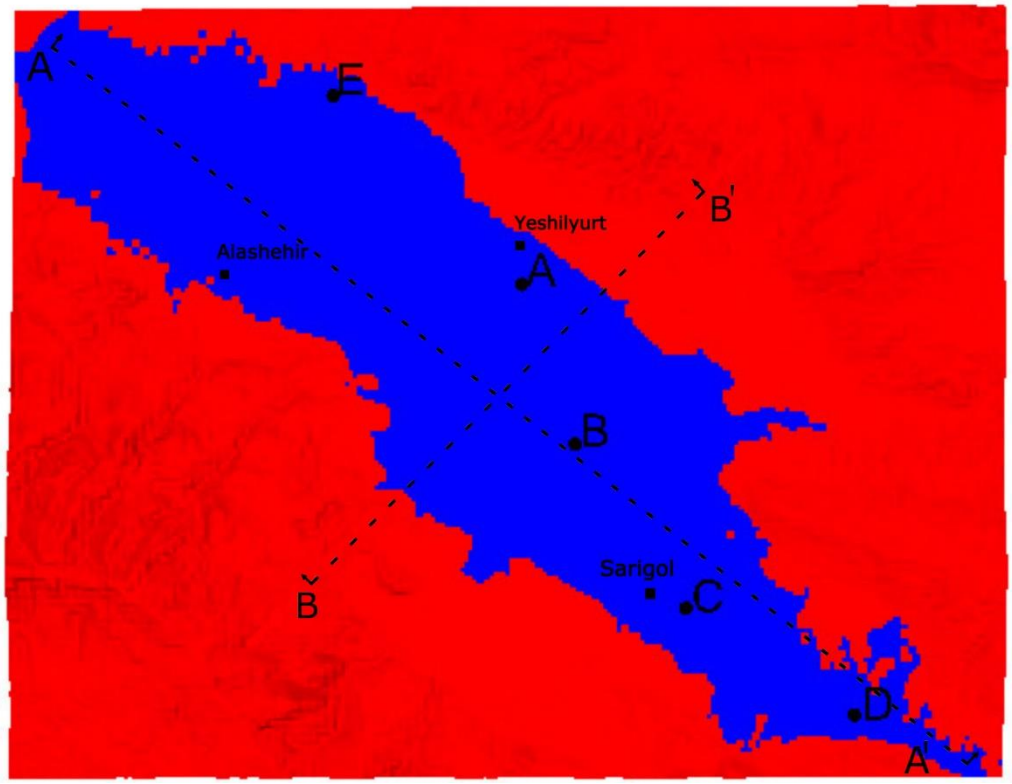

Figure 5- 4 The study area with the 5 nodes (A-E) and the traces of the two vertical sections (AA', BB') where the GEPSD results are presented

Figures 5-4 to 5-7 show the distribution of the vertical movement of the land surface in September and April 2015, 2017, 2019, and 2021. The highest subsidence value was around 4 m.

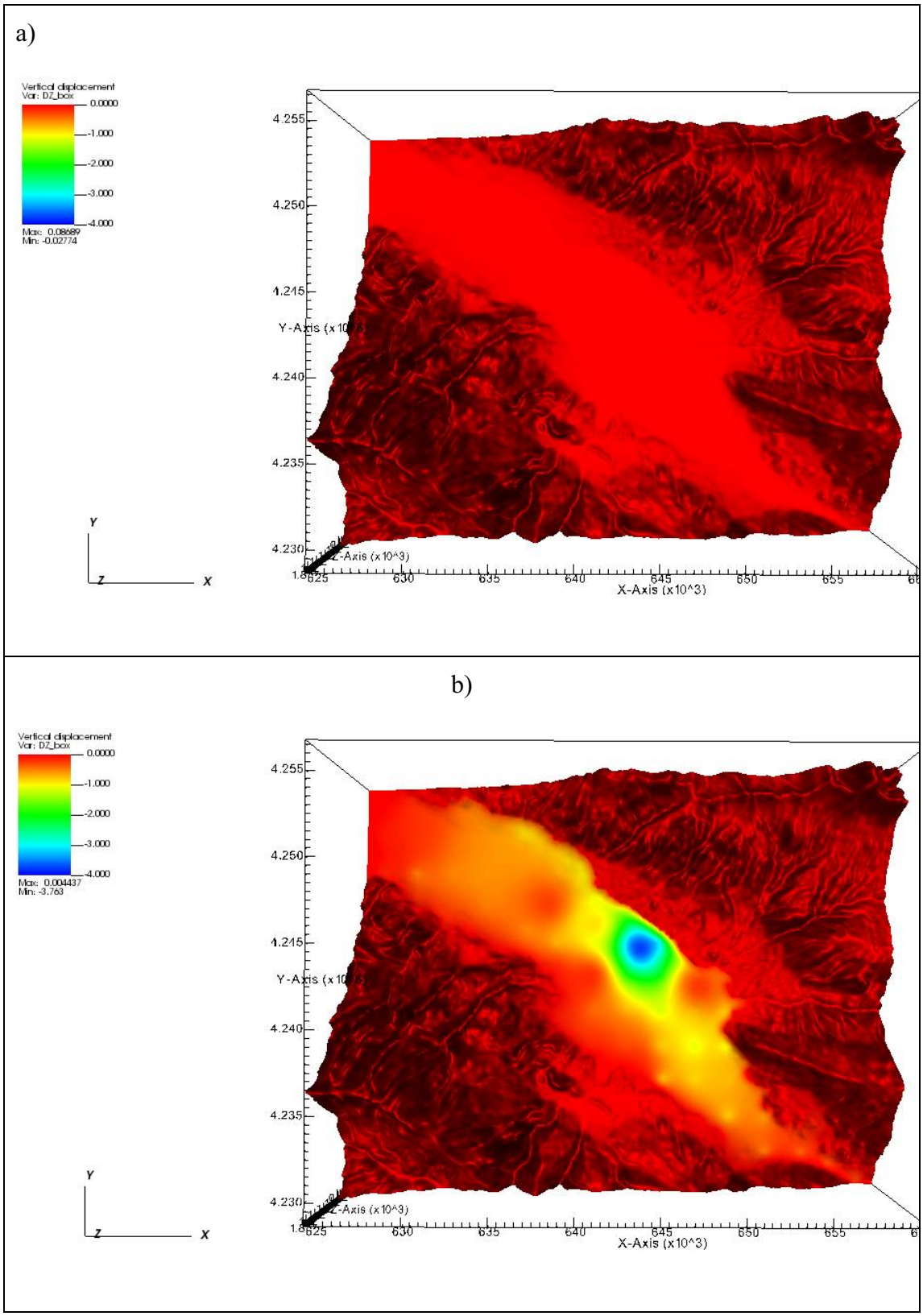

Figure 5- 5 Vertical land displacement as computed by GEPS3D for the GRB in a) April and b) September 2015.

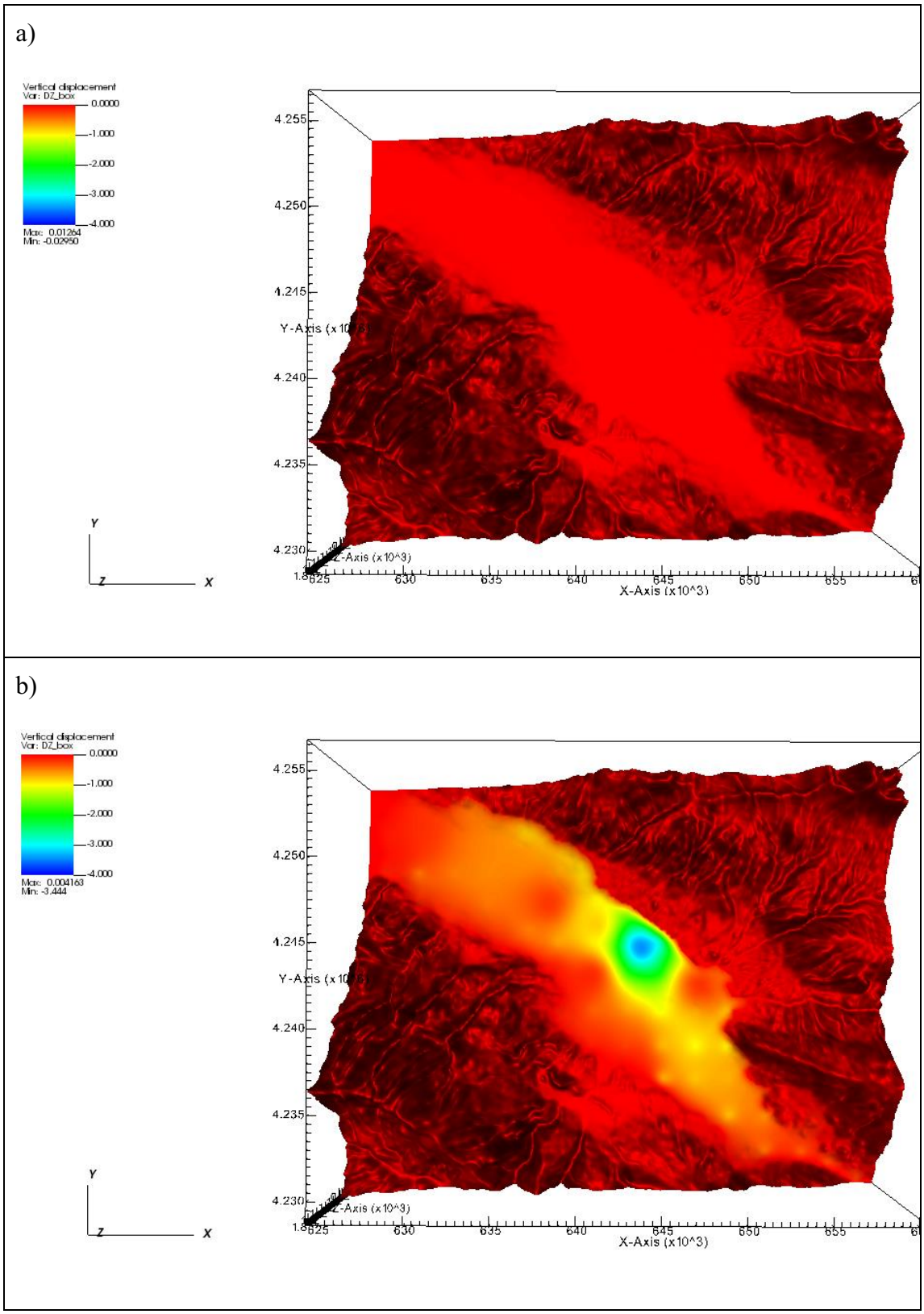

Figure 5- 6 Vertical land displacement as computed by GEPS3D for the GRB in a) April and b) September 2017.

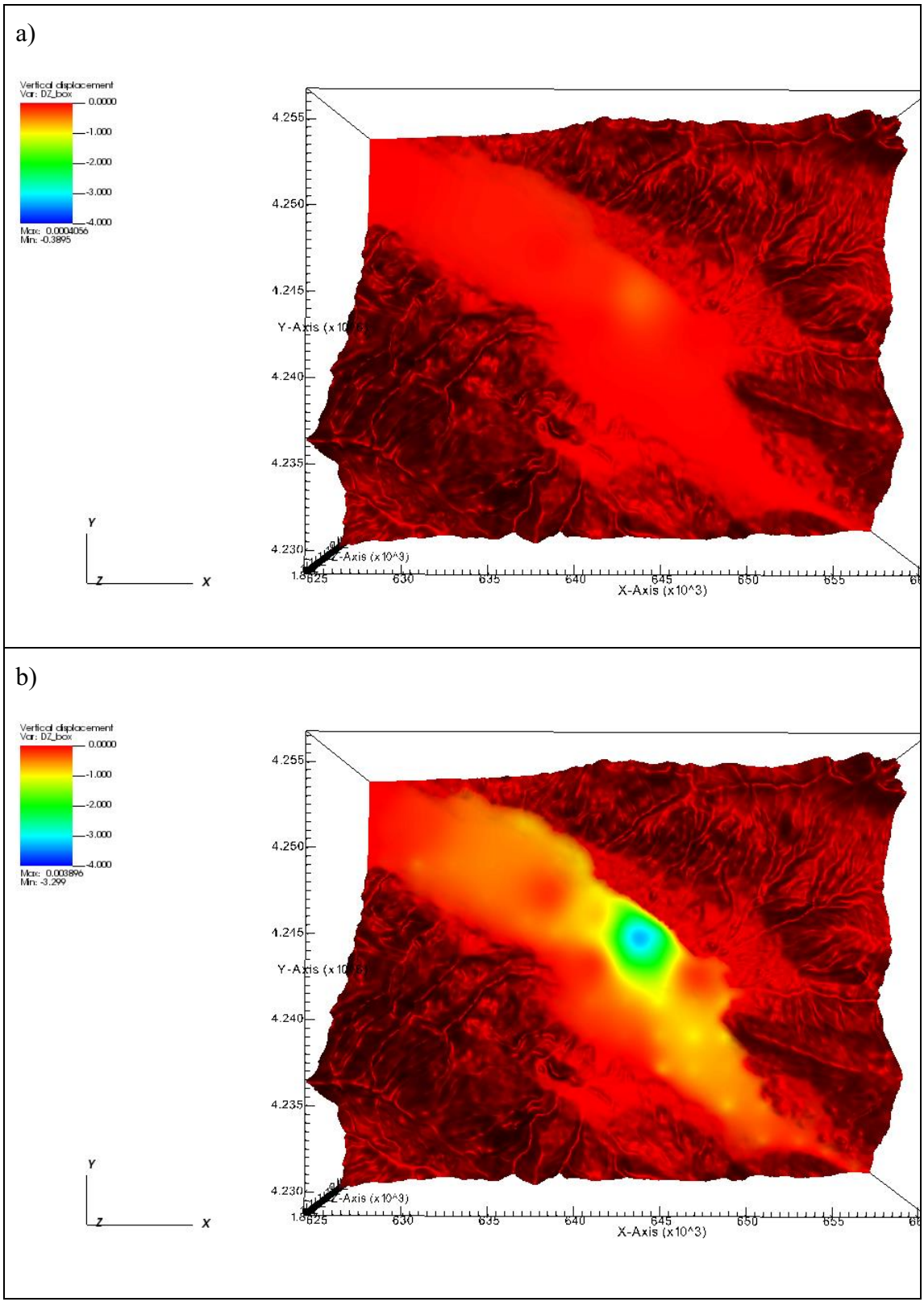

Figure 5- 7: Vertical land displacement as computed by GEPS3D for the GRB in a) April and b) September 2019

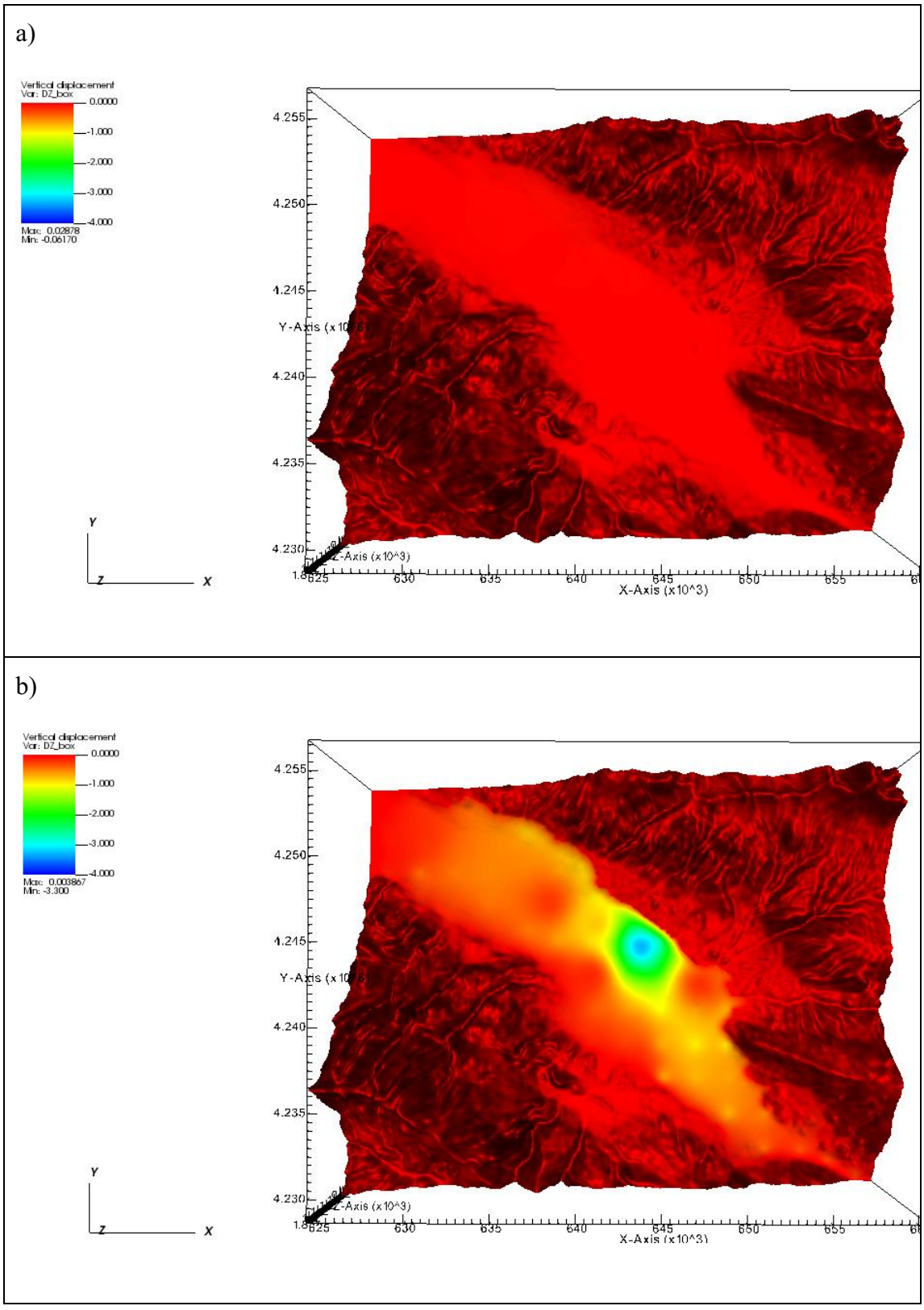

Figure 5- 8 Vertical land displacement as computed by GEPS3D for the GRB in a) April and b) June 2021.

Starting from the driest period of 2015 (Figure 5-4) land subsidence affected the Allasehir alluvial plain in the East part of the region. Also the area surrounding Yeshilyurt region (see Figure 5-3) was affected by land subsidence, with values up to 3 m. As it was mentioned before in the ModelMuse result, the direction of groundwater flow is from the southeast to the northwest. Some areas in the southern Sarigol region experienced slight subsidence of up to approximately 1 m, while no vertical displacement was observed in the northern Alasehir region. In 2017 (Figure 5-5), a certain reduction in land subsidence was observed. The Yesilyurt region experienced a decrease in vertical displacement from 3.7 to 3.4 m, and the Sarigol region showed land uplift of up to 0.5 m.

In 2019, land subsidence continued to decrease, though less significantly. Yesilyurt region experienced a decrease in 0.5 meters. Surrounding areas also shows decrease of subsidence in 2017. Compared to 2015 it changed from 2.9 m to 2.6 m, and from 1.9 m to 1.6 m. The lower part of the region also shows some decrease of land subsidence, up to 0.3 m.

In 2021 (Figure 5-7) the result of entire simulation in terms of vertical land displacement (in June 2021) is shown. All the regions are characterized by a land subsidence similat to that of the corresponding season in 2017. This may indicate that the recovery of hydraulic pressure has slowed down, and that additional measures may need to be taken to further mitigate land subsidence in the region.

In wet periods (Figure 5-4, Figure 5-5, Figure 5-6, Figure 5-7) of the year the recovery of the pressure head caused a large uplift of the land surface that almost return

to its initial elevation. Obviously, this is not physical, but is due to the fact that, consistently with the flow model, the mechanical hysteresis was neglected in these preliminary analyses.

Figure 5-8 and Figure 5-9 show the vertical displacement along the vertical cross section of A-A' crossing the model domain from South to North in April and September 2015 (Figure 5-8) and April-June 2021 (Figure 5-9). The figures allow to understand which layers have been subjected to vertical displacement.

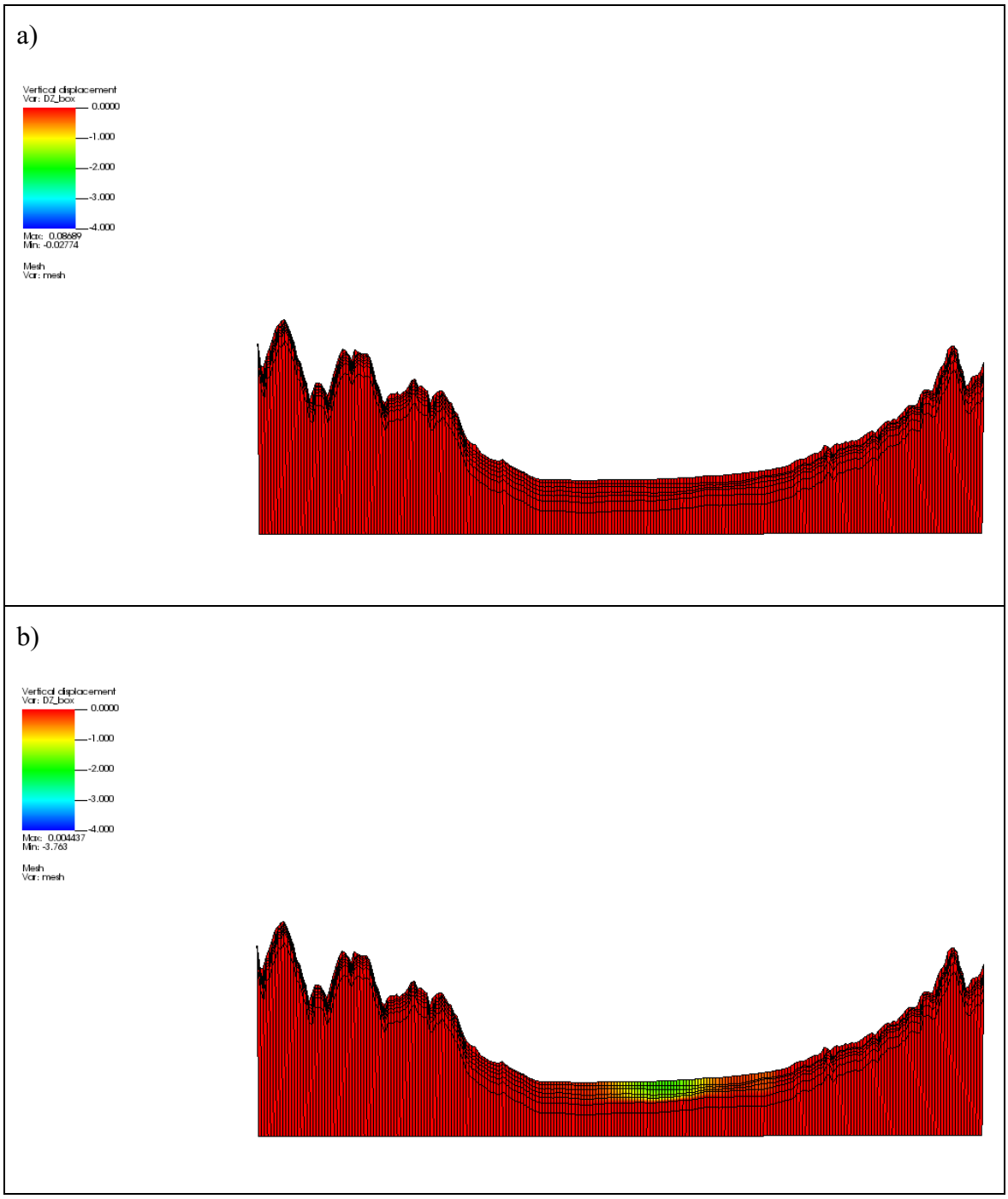

Figure 5- 9 Vertical section A-A' of the model domain with the distribution of the vertical displacements in a) April and b) September 2015 as provided by GEPS3D.

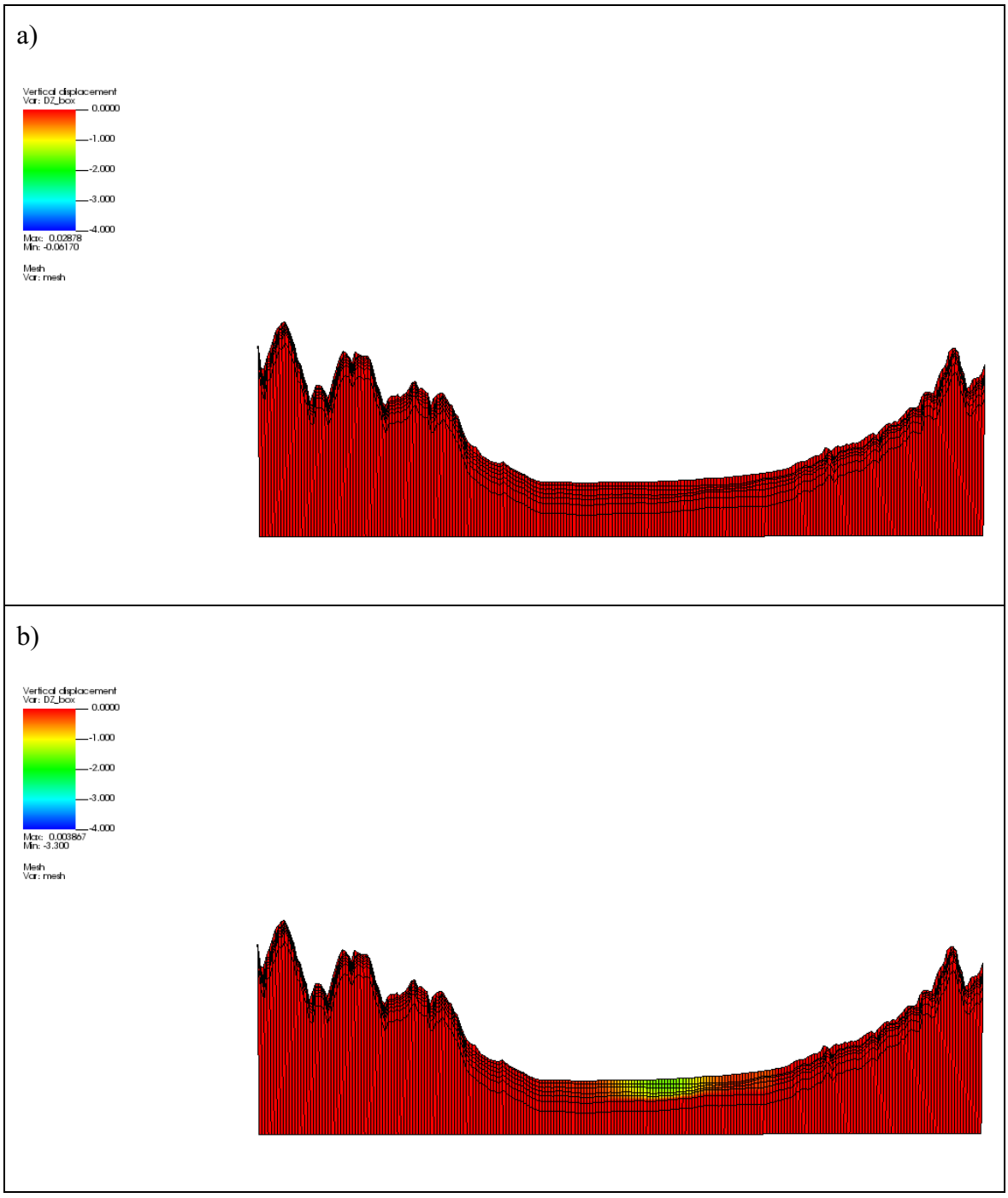

Figure 5- 10 Vertical section A-A' of the model domain with the distribution of the vertical displacements in a) April and b) June 2021 as provided by GEPS3D..

From the Figures 5-9 it is possible to observe that:

-The subsidence occurred in the upper layers of the aquifer system of the study model, which are composed of relatively loose, unconsolidated sediments that are more susceptible to compaction under hydraulic pressure changes.

-The deeper layers, which are composed of more consolidated rock or clay formations, were less affected by compaction.

-The extent and severity of the subsidence varied spatially, with the highest rates of subsidence occurring in the Yeshilyurt region and gradually decreasing in magnitude.

GEPS3D also computes the horizontal land displacements along the West-East and South- North-South reference directions. Based on the reference directions, the analysis of horizontal land displacements must be developed taken into account that:

- along the x-axis, a positive value indicates a movement of the land to the east, negative values indicate a movement westward;

- along the y-axis, a positive value indicates a movement of the land to the north, and negative values represent southward displacements.

Figures 5-10 to 5-17 show the West-East and South-North land displacements movements as computed by GEPS3D at the surface of the model domain in April and September 2015, 2017, 2019 together with April and June 2021.

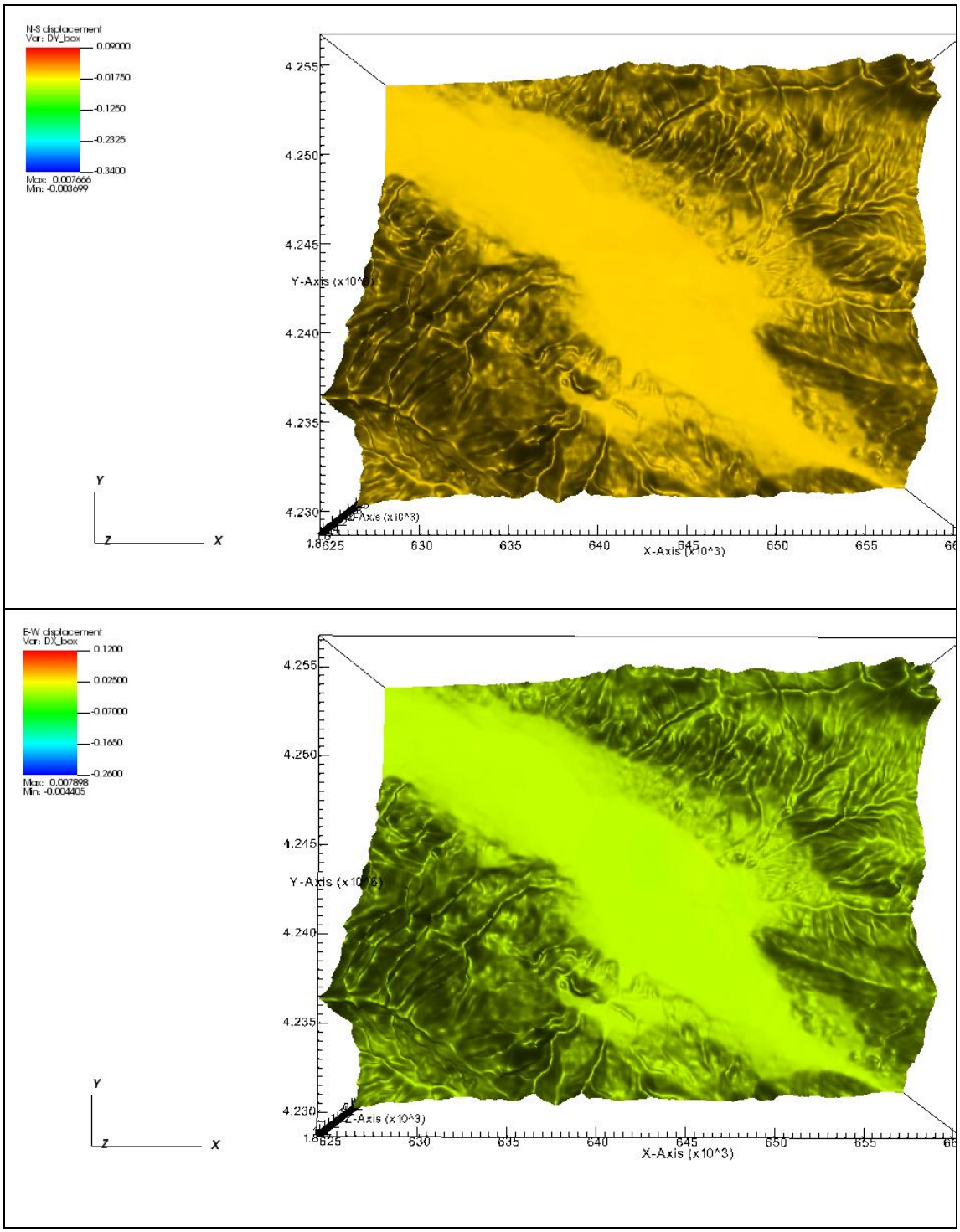

Figure 5- 11: a) West-East-and b) South-North land displacements in April 2015 as simulated by GEPS3D

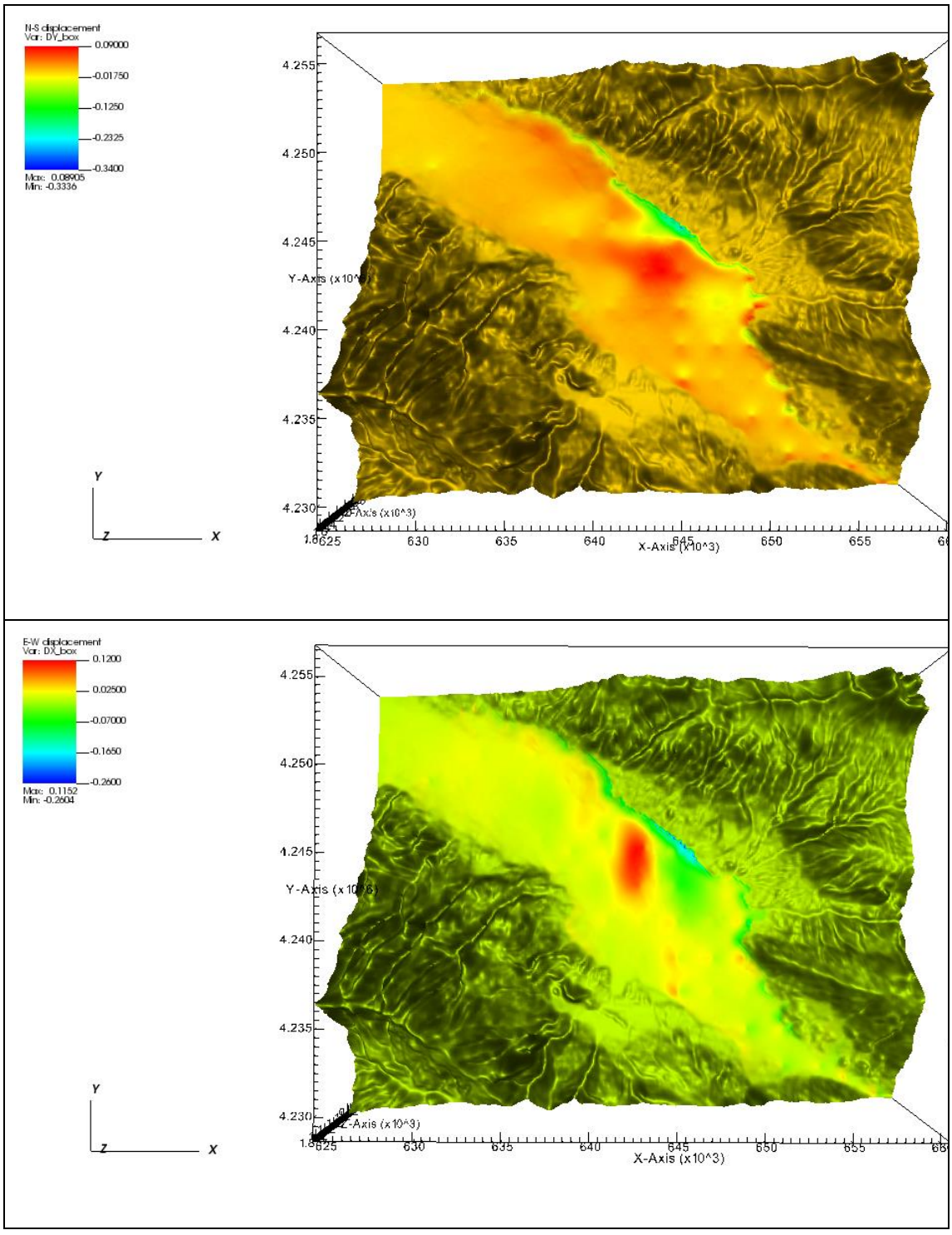

Figure 5- 12: a) West-East-and b) South-North land displacements in September 2015 as simulated by GEPS3D

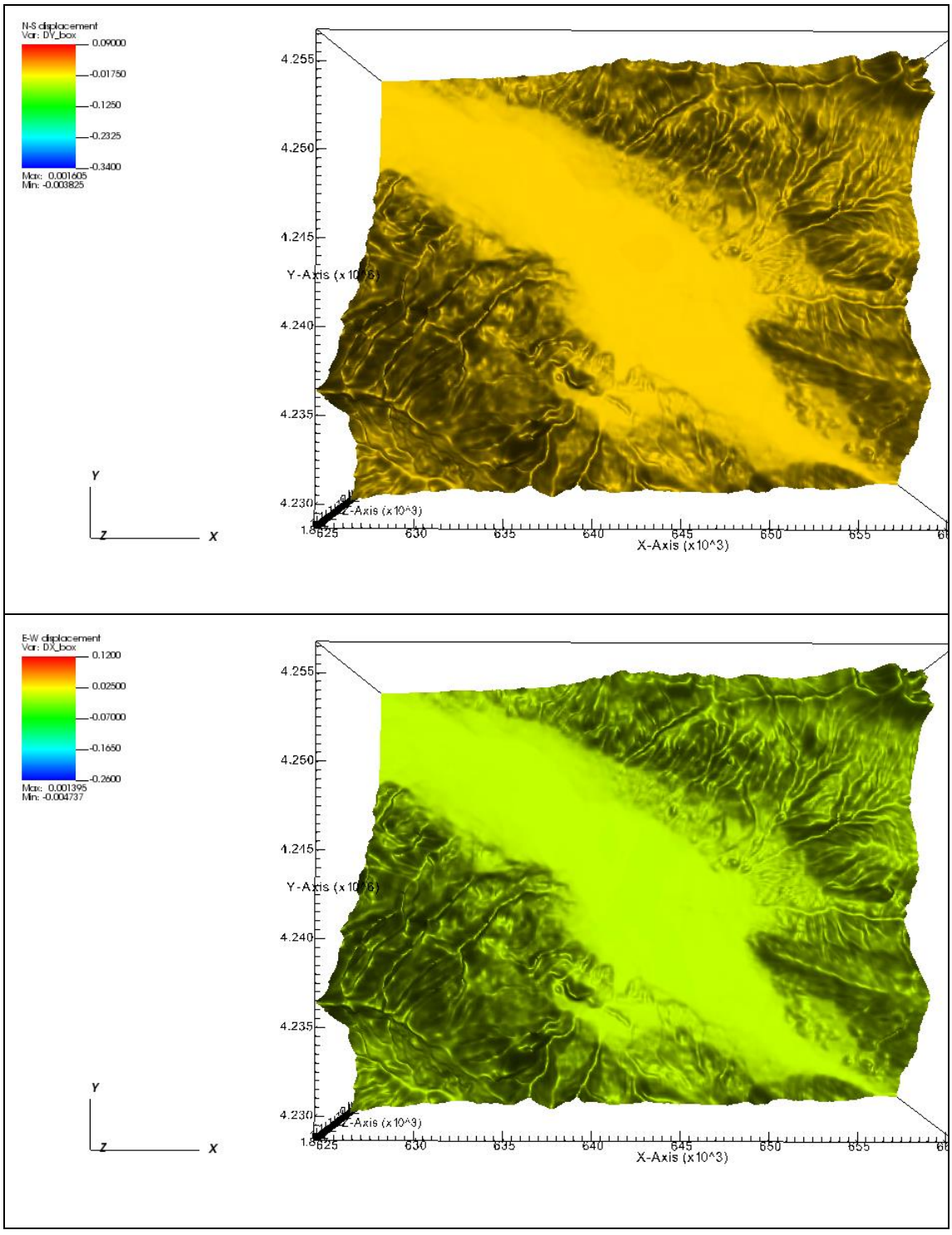

Figure 5- 13: a) West-East-and b) South-North land displacements in April 2017 as simulated by GEPS3D

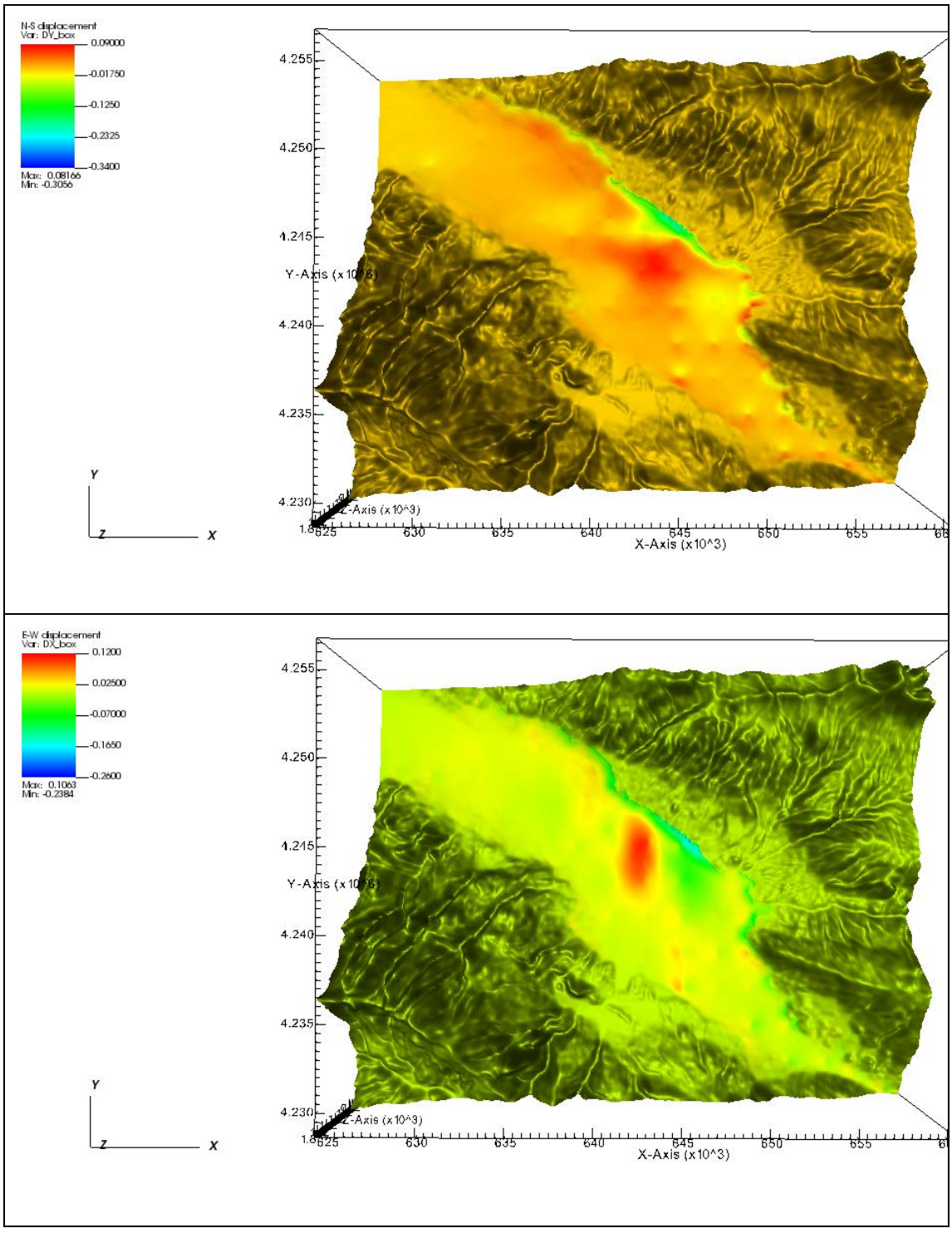

Figure 5- 14: a) West-East-and b) South-North land displacements in September 2017 as simulated by GEPS3D

The displacements in Figure 5-10 refers to April 2015, which was a wet period. Consistently, the figure shows a relatively small displacement in West-East directions, indicating that the land surface was moving slightly in both directions. The South-North displacement was similarly small. This suggests that during a wet period, the groundwater levels in the aquifer system were higher, and therefore the degree of land movement was lower. In contrast, the displacement values for the driest period show a much larger West-East displacement, indicating that the land surface was moving in some areas and significantly in others. The North-South displacement was also relatively large.

The displacement values (Figure 5-12) for wettest period of 2017, were similar to those in April 2015, indicating that the degree of land subsidence was relatively low during this time. The displacement values for September, which was another dry period, were also similar to those in 2015, indicating that the degree of land subsidence was once again greater during a dry period. The largest displacement values occurred during the driest period, which suggests that the lowering of the piezometric levels due to groundwater pumping had a greater impact on land subsidence during times of low water availability. This is likely because during dry periods, the aquifer system is already under stress, and additional pumping exacerbates the situation, leading to greater subsidence.

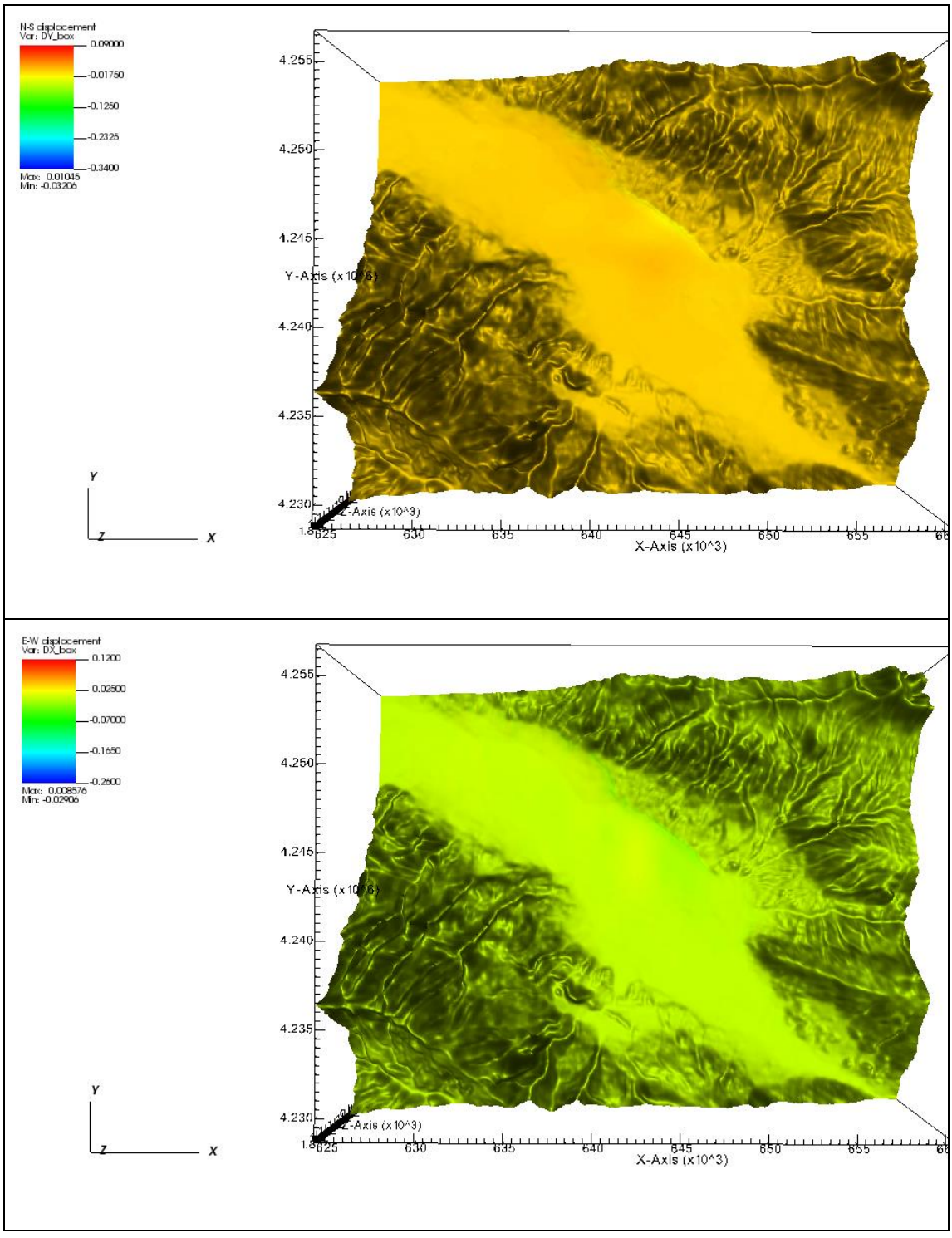

Figure 5- 15: a) West-East-and b) South-North land displacements in April 2019 as simulated by GEPS3D

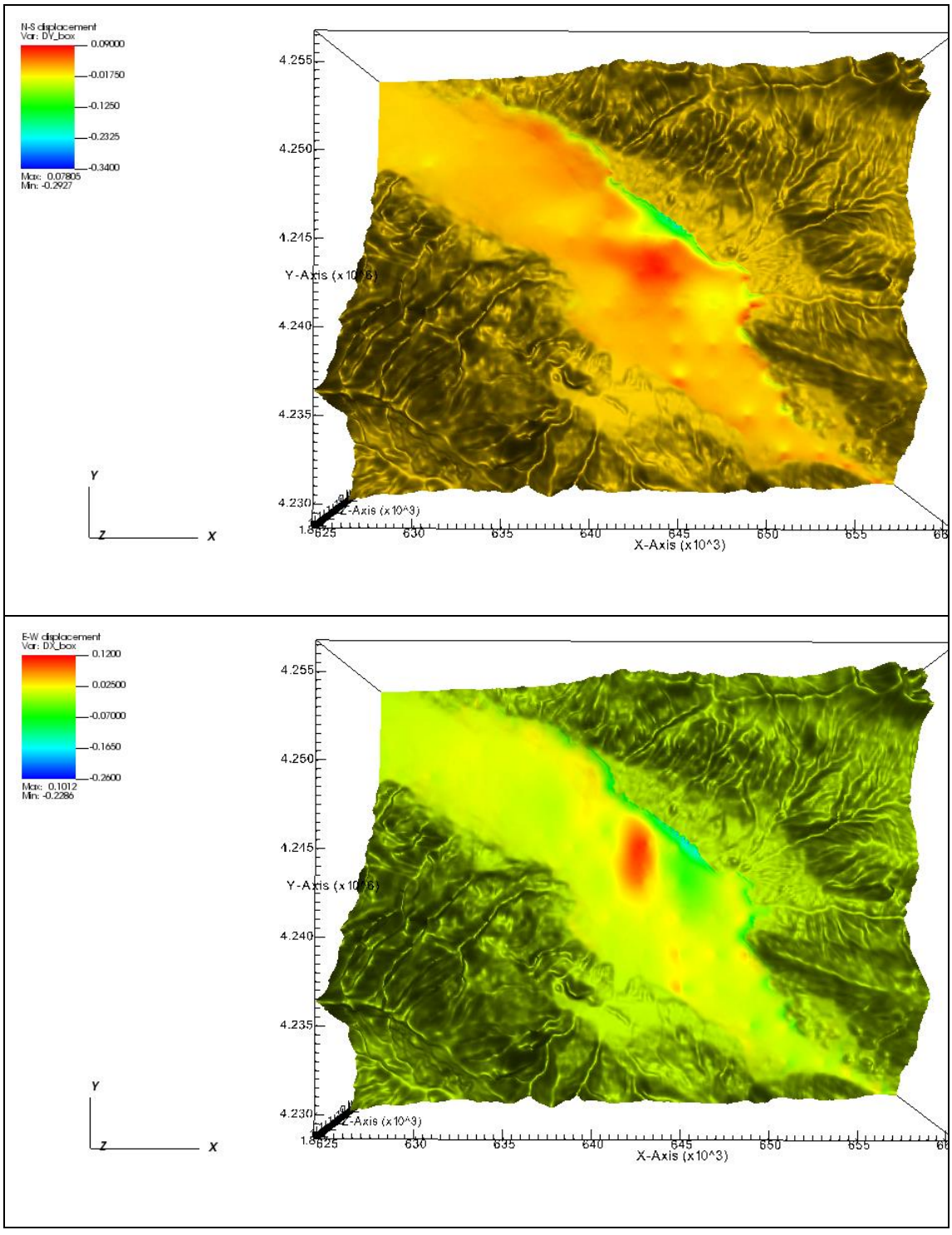

Figure 5- 16: a) West-East-and b) South-North land displacement in Septembers 2019 as simulated by GEPS3D

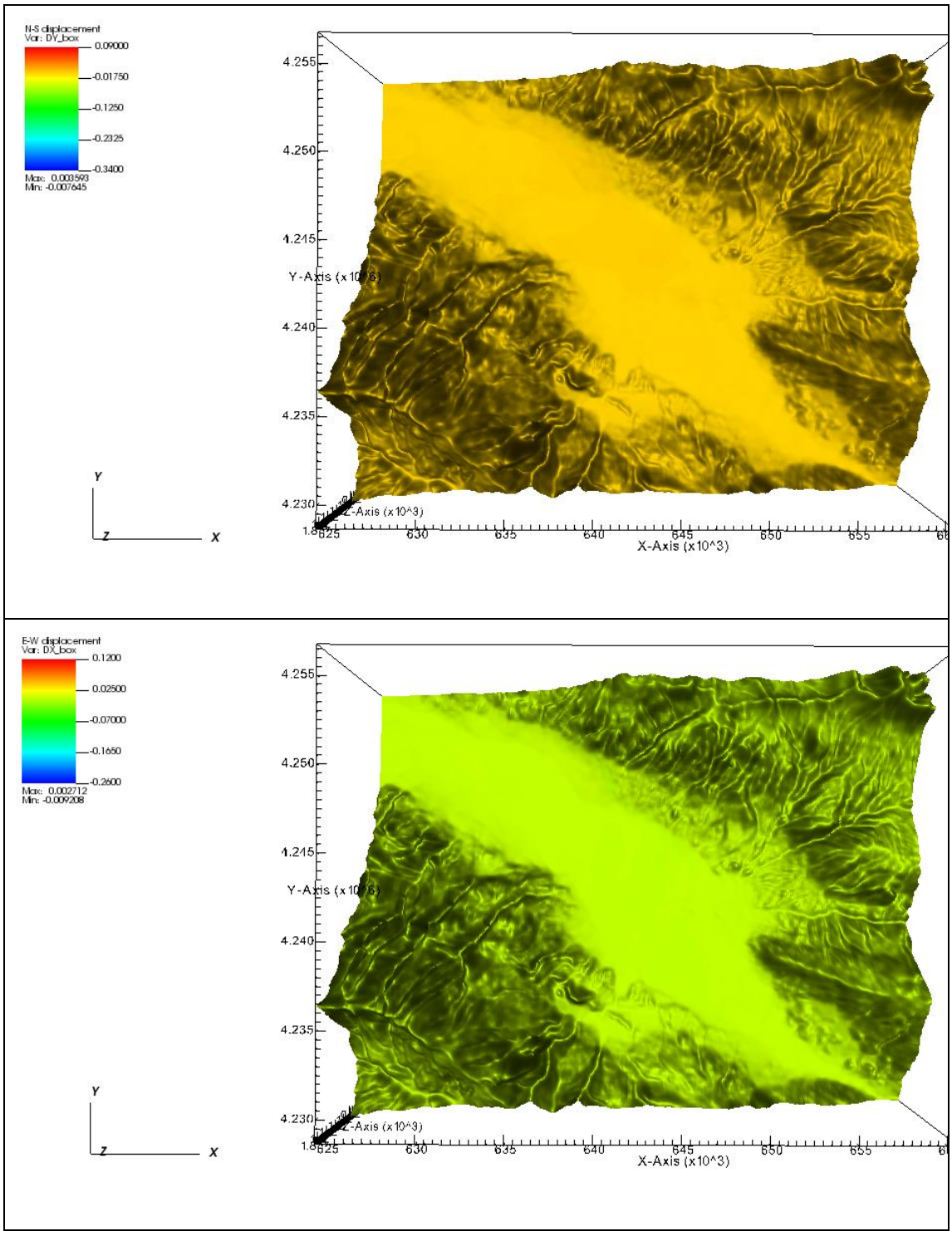

Figure 5- 17: a) West-East-and b) South-North land displacement in April 2021 as simulated by GEPS3D

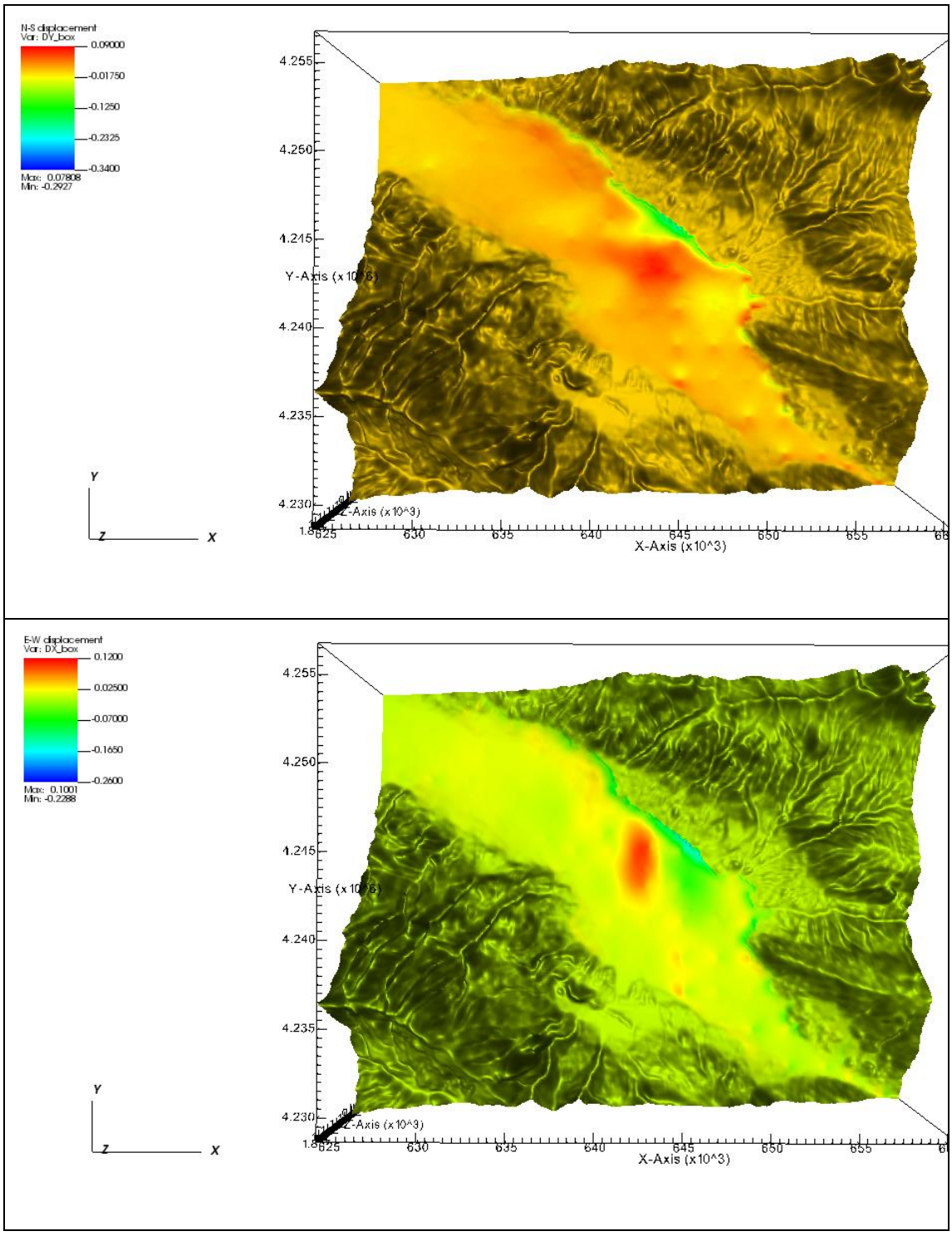

Figure 5- 18: a) West-East-and b) South-North land displacements in June 2021 as simulated by GEPS3D

In the Figure 5-14, values for wet period in 2019, presents a relatively small E-W displacement. The N-S displacement was slightly larger. The displacement values for

September 2019 shows a much larger E-W displacement of 0.1 and -0.22 m, indicating that the land surface was significantly moved in some areas. The N-W displacement was also relatively large at 0.07 and -0.29 m. Compared to the past results in the dry period, E-W displacement decreased , for N-S also decrease but slightly. In 2021 the displacement values were small, for April indicates that the land surface was only slightly moved. The South-North displacement was similarly small at 0.007. The values for June 2021, which was the last month of simulation period, show a much larger West-East displacement of 0.1 and -0.23 m, indicating that the land surface significantly moved. The South-North displacement was also relatively large at 0.07 and -0.29 m.

Overall, these results suggest that horizontal land subsidence is occurring in the study area and that the degree of subsidence is greater during dry periods when groundwater pumping is likely to be highest. The displacement values for 2015 and 2017 show that the degree of land subsidence was also affected by the wet and dry periods in those years. The displacement values for the last two years of your simulation period (2019-2021) show that the degree of land subsidence has continued, but with smaller displacement values during wet periods than in previous years.

Figures from 5-18 to 5-21 show the model outcome along the vertical sections B-B' whose traces are presented in Figure 5-3. Land displacements were reported in 2015 and 2021. Horizontal displacements help to understand the underlying processes that are causing the displacement, such as faulting, subsidence, or ground deformation due to changes in groundwater levels.

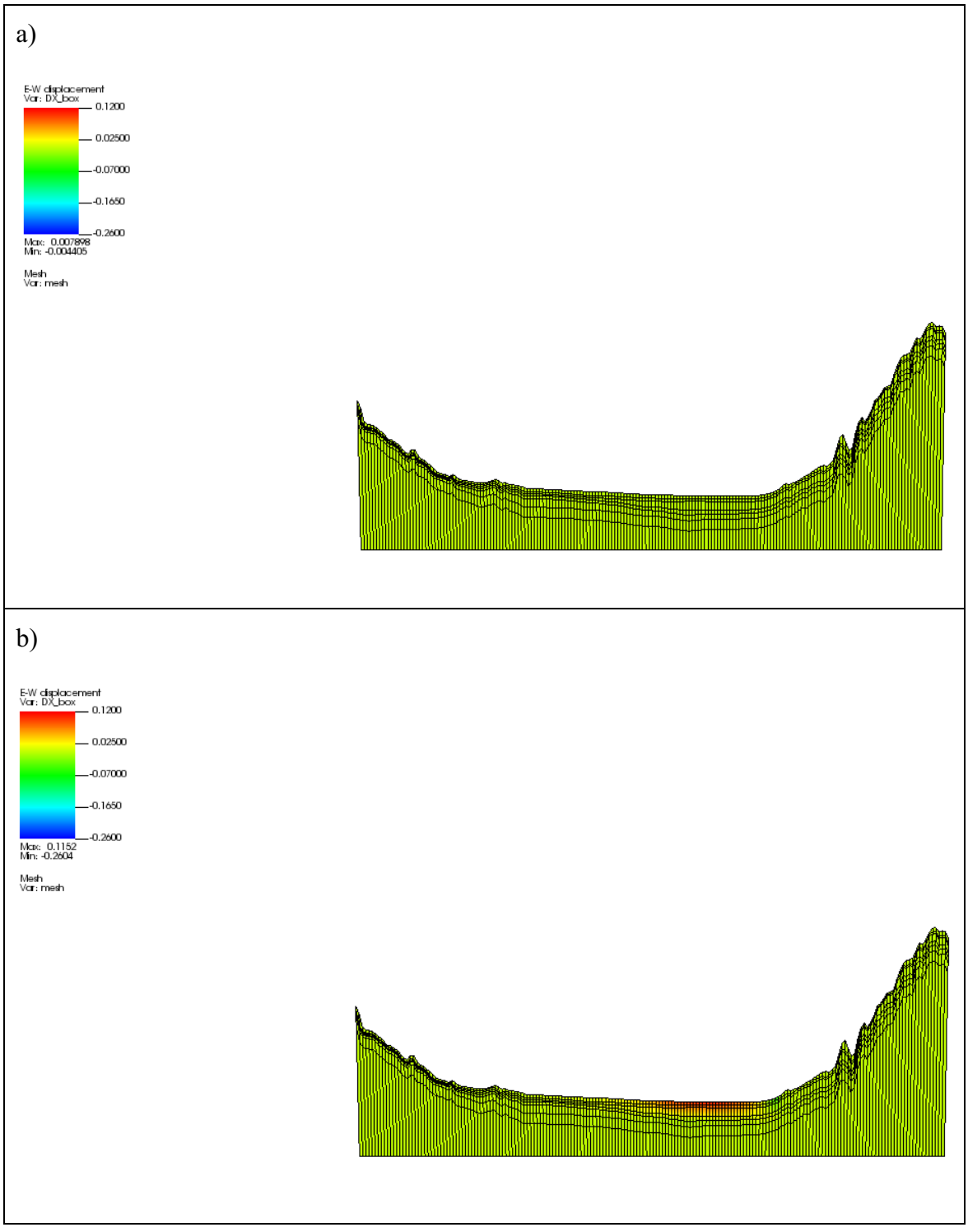

Figure 5- 19: West-east horizontal displacement in a) April and b) September of 2015, along the B-B' cross section, as simulated by GEPS3D

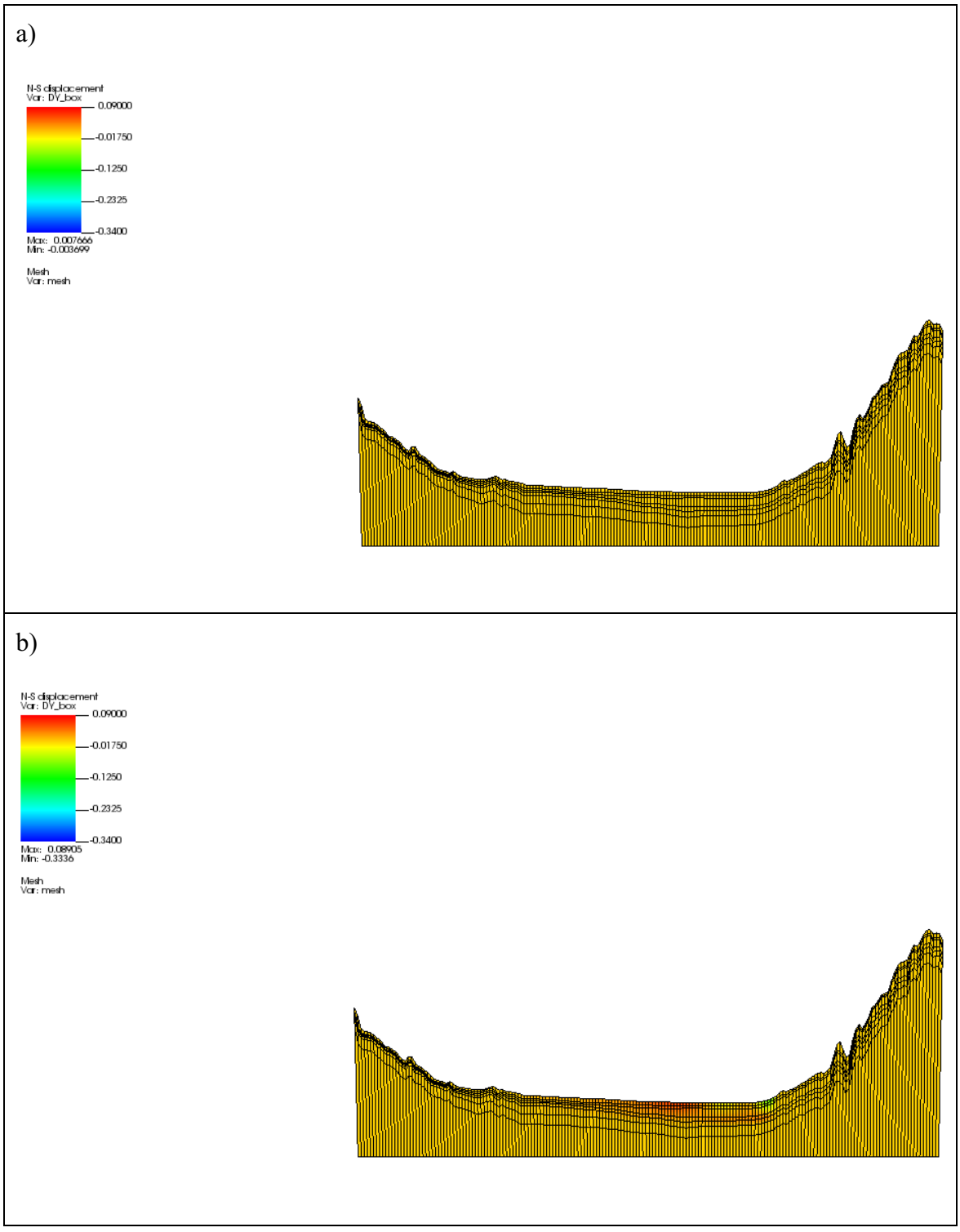

Figure 5- 20: South-North horizontal displacement in a) April and b) September of 2015, along the B-B' cross section, as simulated by GEPS3D

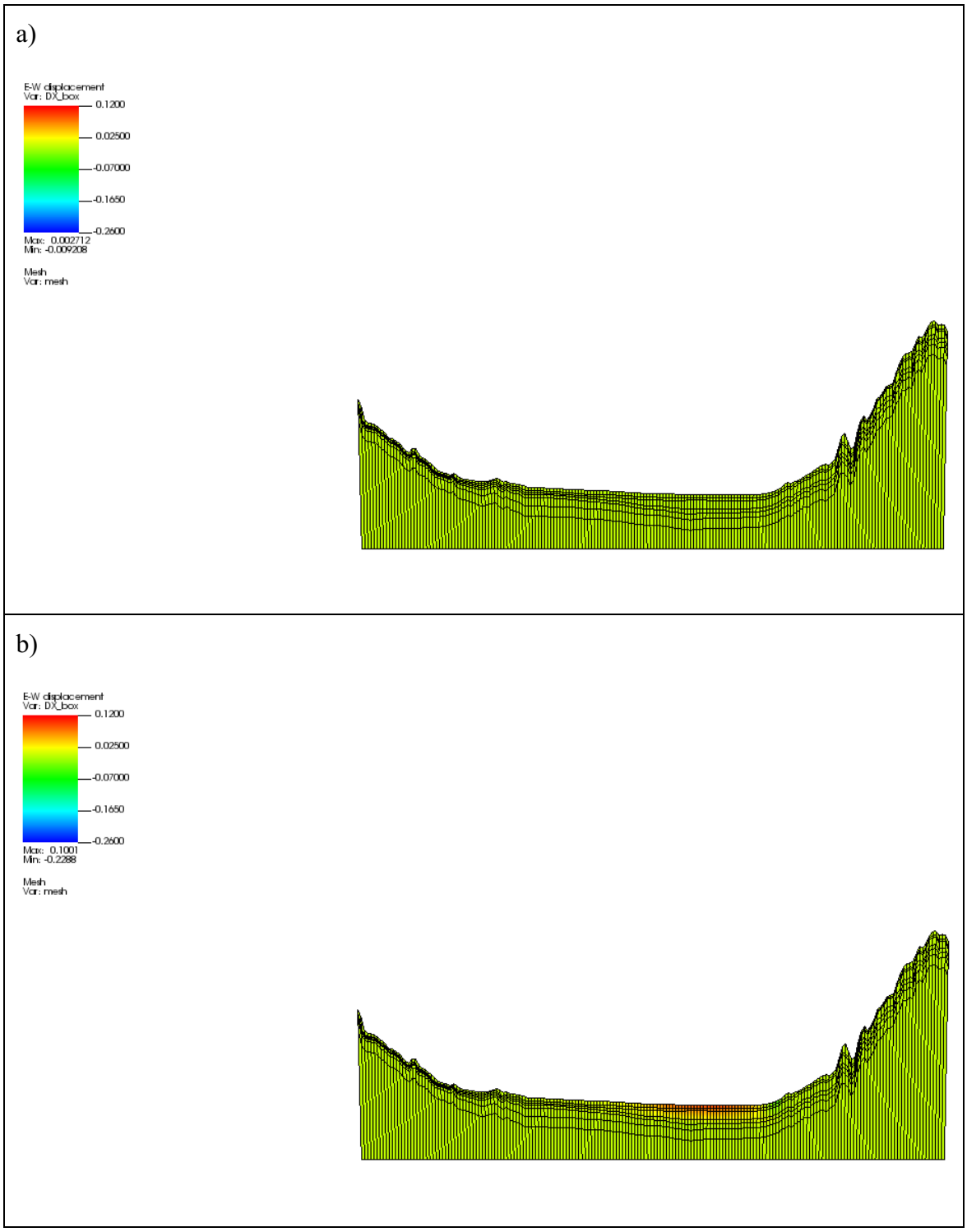

Figure 5- 21: West-east horizontal displacement in a) April and b) June of 2021, along the B-B' cross section, as simulated by GEPS3D

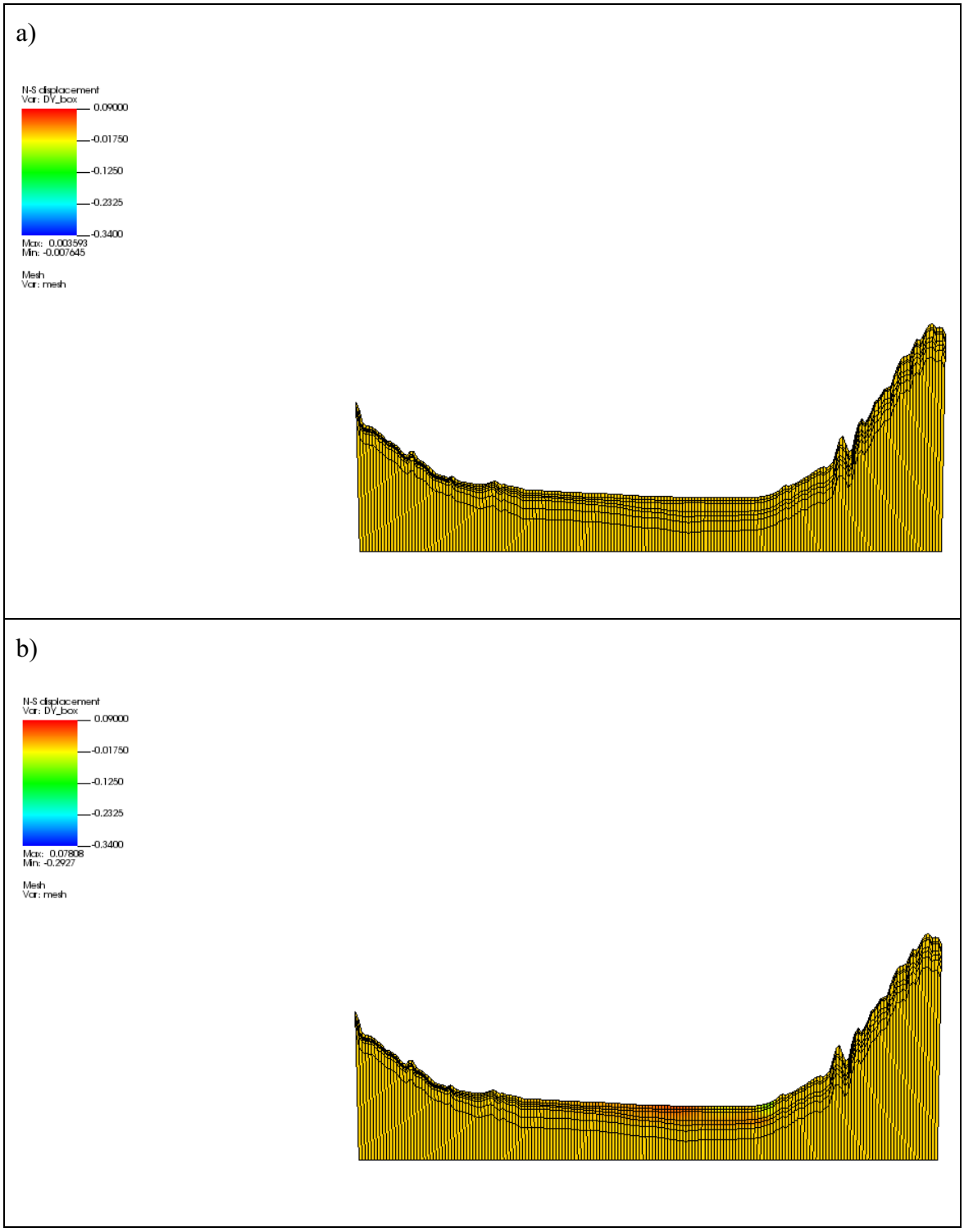

Figure 5- 22: South-North horizontal displacement in a) April and b) June of 2021, along the B-B' cross section, as simulated by GEPS3D

In terms of the specific layers that are affected by land displacement (Figures 5-18 to 5-20) it is likely that the shallower layers of the aquifer system are more susceptible to horizontal displacements. Additionally, the specific lithology of the aquifer system may also influence which layers are more prone to subsidence. For example, layers composed of softer, more compressible sedimentary deposits may experience greater deformation than harder, more resistant rock layers.

The GEPS3D solution has been also visualized in terms of behavior versus time of the various displacement components at a number of selected locations (nodes A to F in Figure 5-3) over the whole period from October 2013 to June 2021. Figures from 5-22 to 5-26 provide the behavior of land subsidence (a), and horizontal displacements b) West-East and c) South-North of each location over time.

It's should be noticed that the displacement components change significantly over time due to pressure fluctuation. This is mainly related to the elastic constitutive model used in the analysis which neglects mechanical hysteresis. The largest land displacement occurred in the southern part of the GRB region, in correspondence to node A (Figure 5-22a). In the other nodes, which are located in different parts of study area, land subsidence and horizontal displacements are also characterize by a fluctuating behavior with smaller maximum values.

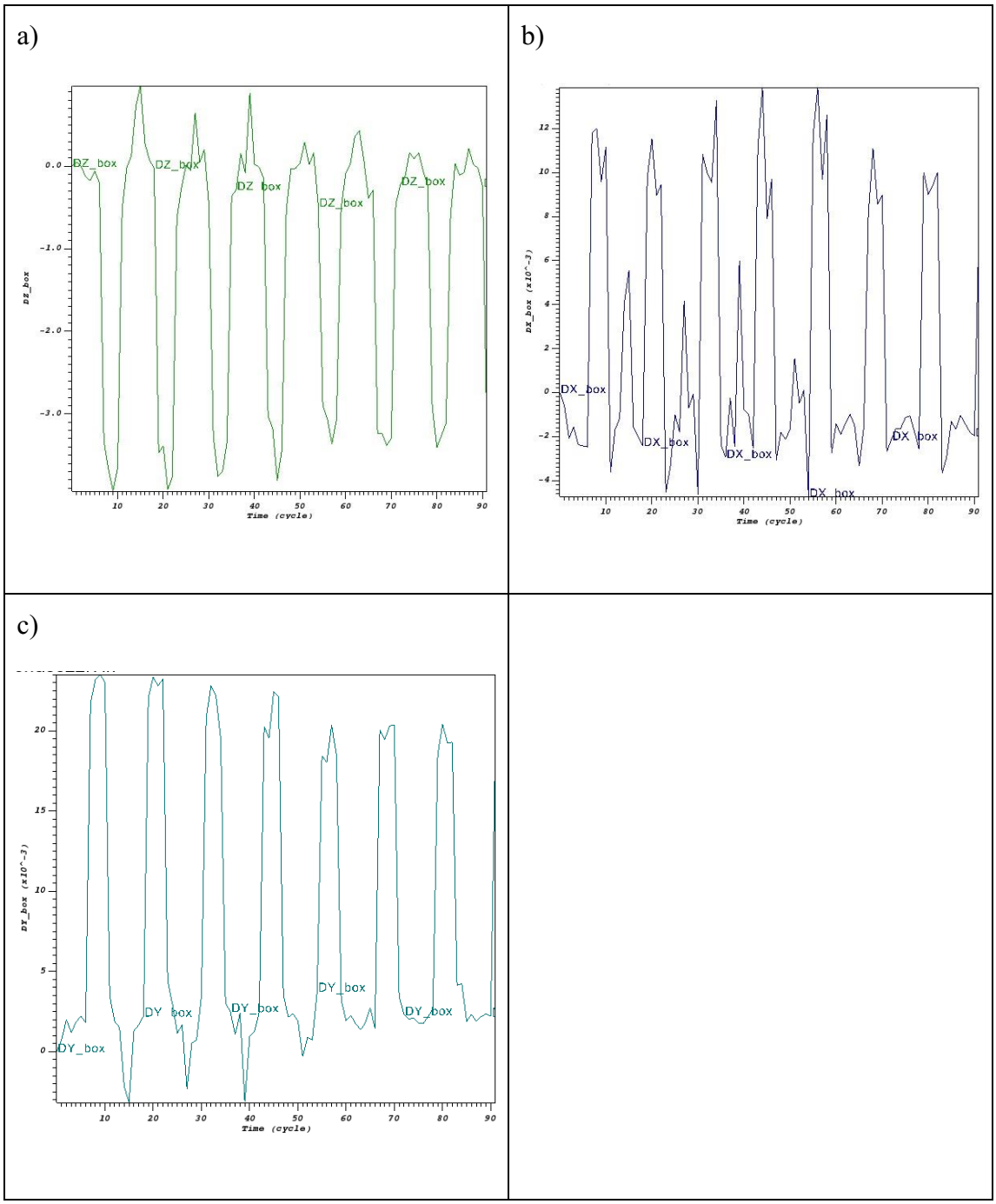

Figure 5- 23: Node A : relationship between time and the behavior of vertical land subsidence (a) calculated by GEPS3D. It also presents data on the East-West (b) and North-South (c) horizontal displacement, both of which were calculated by GEPS3D

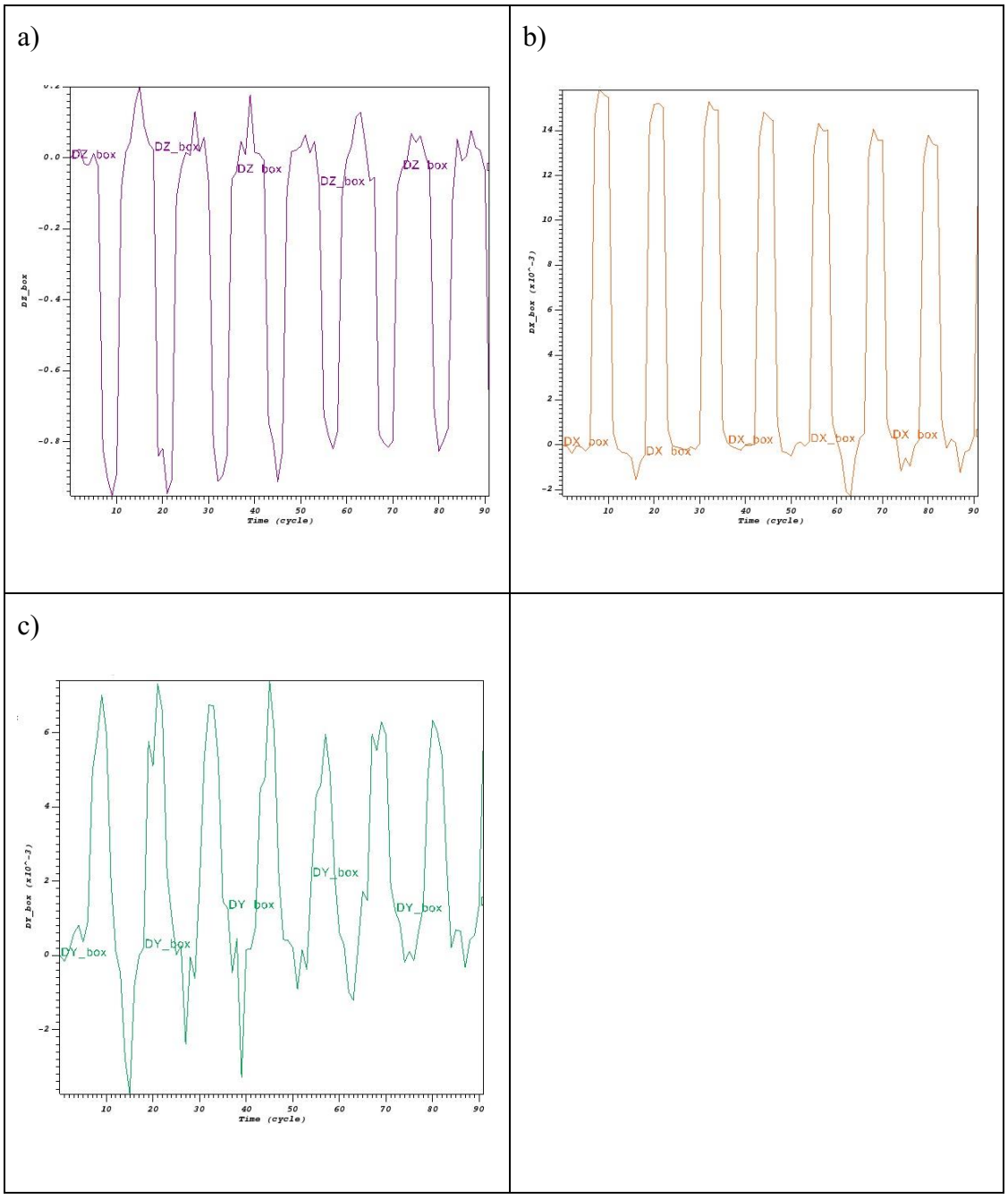

Figure 5- 24: Node B : relationship between time and the behavior of vertical land subsidence (a) calculated by GEPS3D. It also presents data on the East-West (b) and North-South (c) horizontal displacement, both of which were calculated by GEPS3D

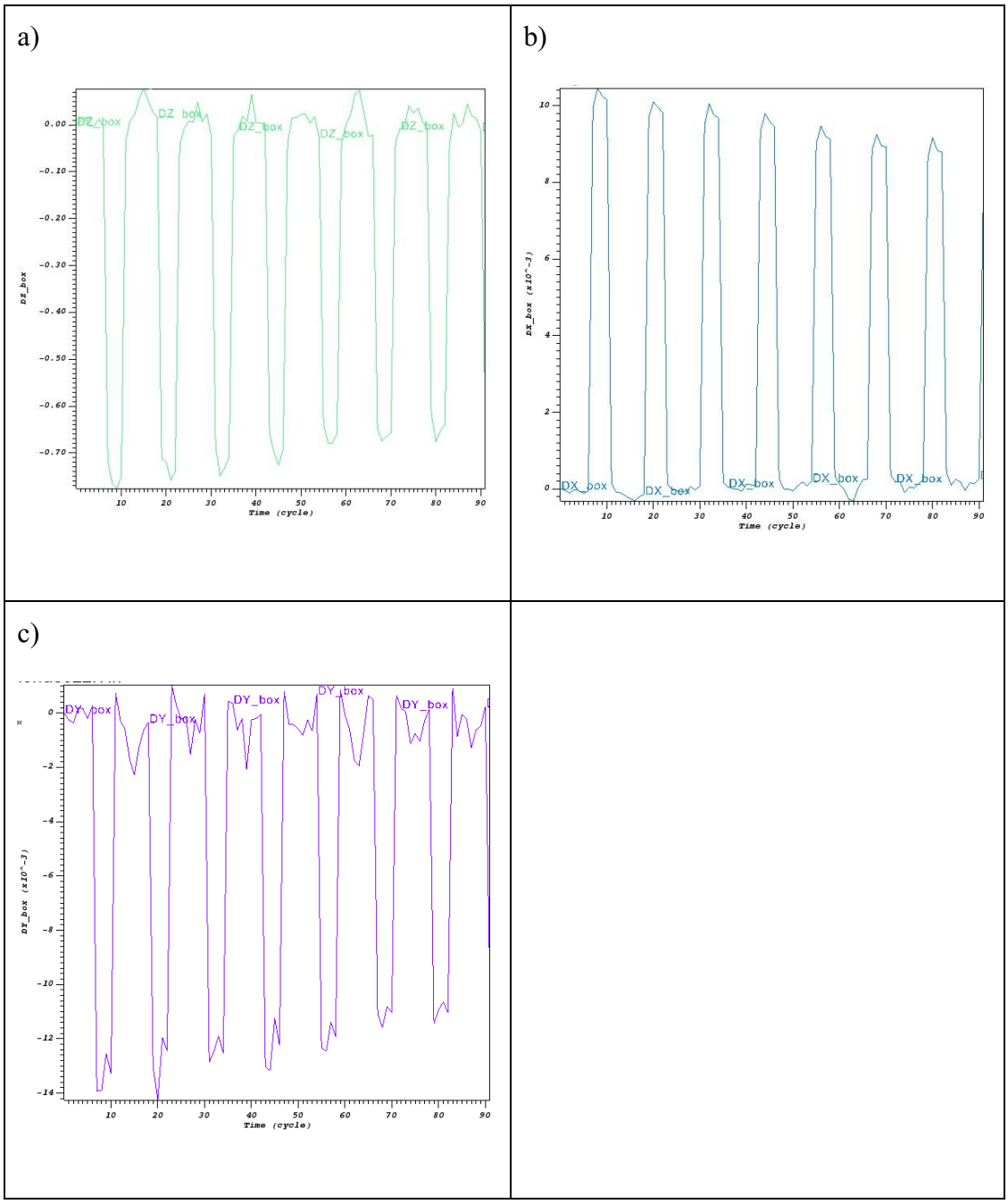

Figure 5- 25: Node C ; relationship between time and the behavior of vertical land subsidence (a) calculated by GEPS3D. It also presents data on the East-West (b) and North-South (c) horizontal displacement, both of which were calculated by GEPS3D)

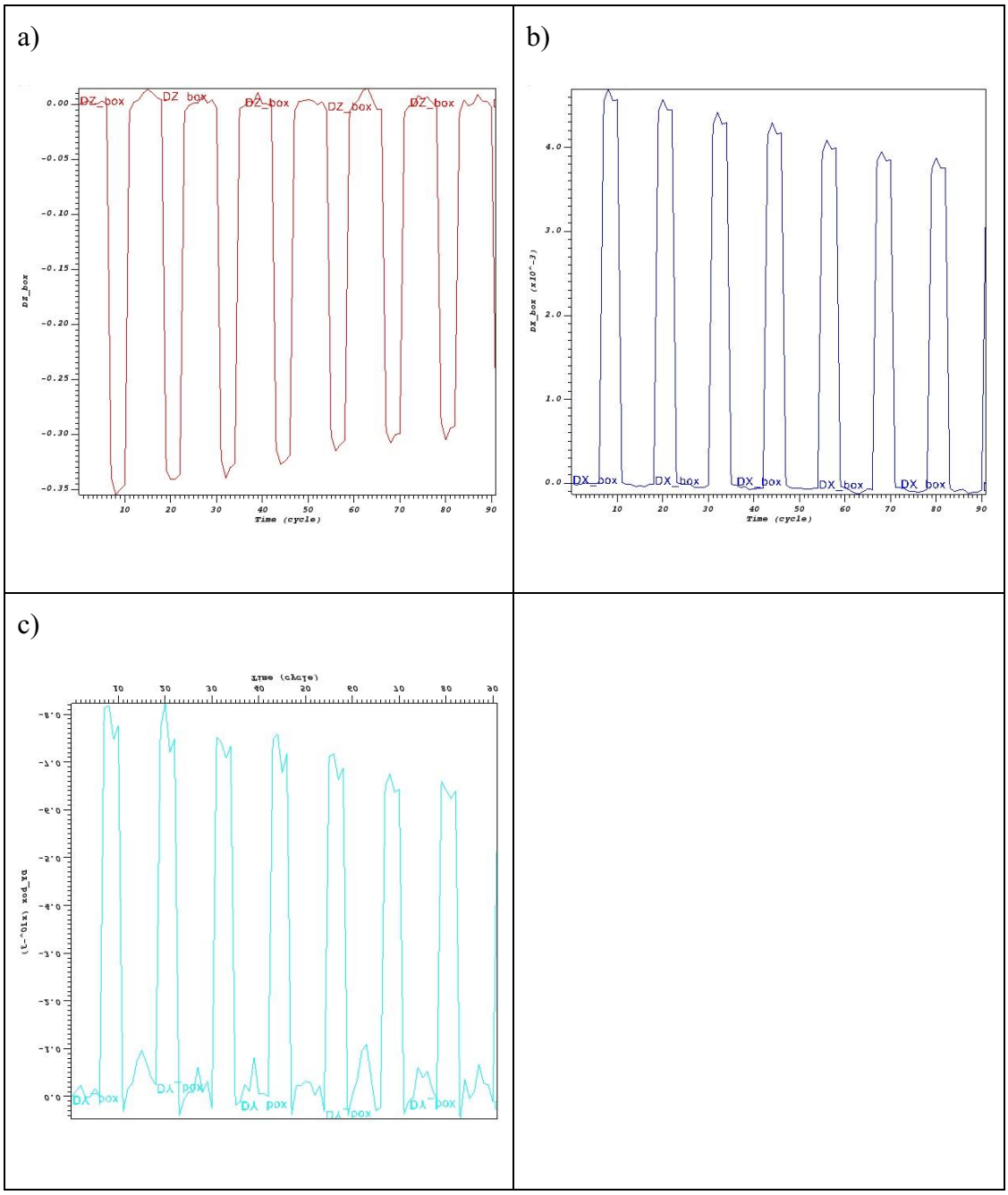

Figure 5- 26: Node D : relationship between time and the behavior of vertical land subsidence (a) calculated by GEPS3D. It also presents data on the East-West (b) and North-South (c) horizontal displacement, both of which were calculated by GEPS3D

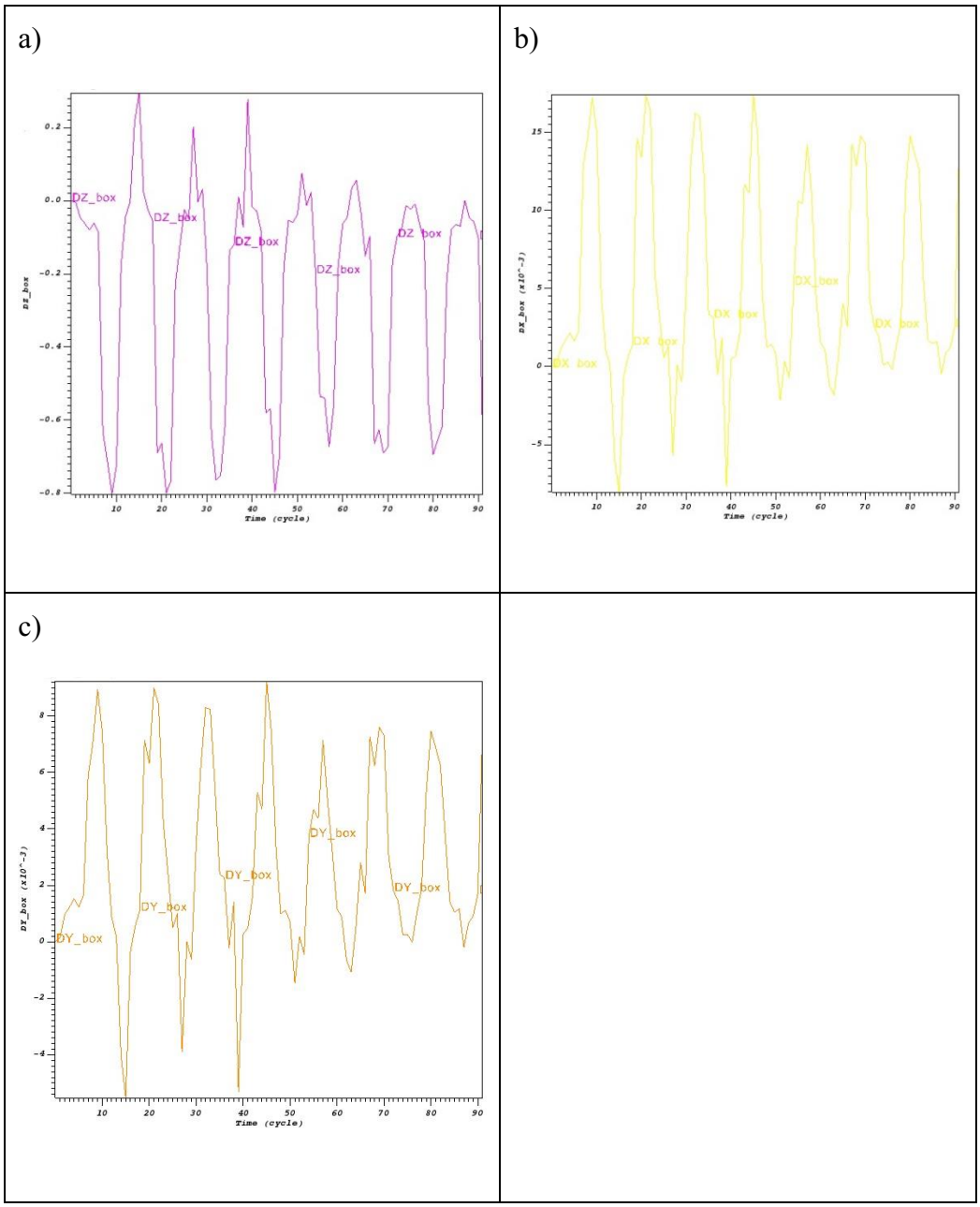

Figure 5- 27: Node E : relationship between time and the behavior of vertical land subsidence (a) calculated by GEPS3D. It also presents data on the East-West (b) and North-South (c) horizontal displacement, both of which were calculated by GEPS3D

Conclusion

The 3D finite-element geomechanical model GEPS3D, developed by the University of Padova, was utilized to investigate the complex dynamics of the aquifer system in the Gediz River Basin. A specialized technique was employed using groundwater flow model data provided by Dokuz Eylul University to obtain both vertical and horizontal displacements, enabling exploration of the entire three-dimensional field of ground motion during entire simulation period (October 2013-June 2021).

The study area experienced land subsidence with the highest value of 4 m in the eastern Allasehir alluvial plain and the surrounding Yeshilyurt region during the driest period of 2015. However, there was a reduction in land subsidence in 2017 and 2019, though the recovery slowed down in 2021. The subsidence occurred mainly in the upper layers of the aquifer system, which are composed of unconsolidated sediments, while the deeper layers, which are composed of more consolidated rock, were less affected by compaction. The severity and extent of subsidence varied spatially, with the highest rates occurring in Yeshilyurt. During dry periods, when pumping is highest and the aquifer system is more under stress, land subsidence is greater. Wet periods, when groundwater levels recover higher values, land subsidence decreases.

It is worth noting that the displacement fields computed in the study underwent significant changes over time following the pressure fluctuations. This is likely unphysical and not supported by the available land subsidence measurement. However, it is caused by the elastic constitutive model employed in the analysis that ignores mechanical hysteresis. Such a choice is forced by the groundwater flow model provided

by Dokuz Eylul University where only elastic storage coefficients were implemented. For this reason, the results here presented must be considered as a preliminary analysis.

The study emphasizes the need for sustainable groundwater management practices to mitigate the impacts of land subsidence, including reducing pumping during dry periods and improving irrigation efficiency. Further research is also needed to better understand the lithology and geology of the aquifer system, as well as the impacts of external factors such as climate change on groundwater availability and land subsidence.

Reference

Alper E., et.al, 2022, Groundwater Flow Model for the Gediz River Basin Alluvial Aquifer (Turkiye)

Anderson, M. P., & Woessner, W. W. (2015). Applied groundwater modeling: simulation of flow and advective transport (2nd ed.). Academic Press.(p.122-124)

Baba A.et al, Blowout mechanism of Alasehir (Turkey) geothermal field and its effects on groundwater chemistry,2016, DOI:10.1007/s12665-016-6334-6

Balasubramanian, A. (2017). Surface water runoff. University of Mysore.

Bru G., et al., A-DInSAR processing in Gediz River Basin (Turkey). Deliverable n.D3.3, RESERVOIR Project, 2021

Custodio, E. Aquifer overexploitation: What does it mean? Hydrogeol. J. 2002, 10, 254–277.

Demirkesen, A. C., Demir, G., Sozbilir, H., & Alpaslan, N. (2019). Estimation of groundwater total recharge and discharge using GIS-integrated water level fluctuation method: a case study from the Alaşehir alluvial aquifer, Western Anatolia, Tury. *Environmental Earth Sciences, 78(23), 1-13*. https://doi.org/10.1007/s12665-019-8734-7\

DSI, 2014. Hydrogeological Study of the Gediz Watershed, Main Report. Eser Project & Engineering Inc.

Erik Stephen Day, Application of the USGS soil-water-balance (SWB) model to estimate spatial and temporal aspects of groundwater recharge in north-central Iowa, 2019

Gabriel B. Senay, et.al, Operational Global Actual Evapotranspiration: Development, Evaluation and Dissemination,2020,DOI:10.3390/s20071915

Gambolati, G.; Teatini, P. Geomechanics of Subsurface Water Withdrawal and Injection. Water Resour. Res. 2015, 51, 3922–3955.

Gambolati, G., Teatini, P. (2021), Land Subsidence and its Mitigation. Published by the Groundwater Project (https://gw-project.org/books/land-subsidence-andits-mitigation/), Guelph, Ontario, Canada.

Lee, C.H., Chen, W.P., and Lee, R.H., 2006, Estimation of groundwater recharge using water balance coupled with base-flow-record estimation and stable-base-flow analysis: Journal of Hydrology, v. 327, p. 564-573.

Nilgun B. Harmancioglua *, Kurt Fedrab , Filiz Barbarosa, (2007) ,Analysis for sustainability in management of water scarce basins: the case of the Gediz River Basin in Turkey

Phien-wej N., et al, 2005, Land subsidence in Bangkok, Thailand, doi.org/10.1016/j.enggeo.2005.10.004

PRIMA Project website: https://reservoir-prima.org/pilot-site-turkey

Rafiei, F., Gharechelou, S., Golian, S., & Johnson, B. A. (n.d.)., Aquifer and Land Subsidence Interaction Assessment Using Sentinel-1 Data and DInSAR Technique,2022, DOI:10.3390/ijgi11090495

Sabater M. J., 2019, ERA5-Land monthly averaged data from 1981 to present. *Copernicus Climate Change Service* (C3S) Climate Data Store (CDS), Accessed 2022-10-06 from https://doi:10.24381/cds.68d2bb30.

Sneed M., et al., 2015, Land subsidence in the San Joaquin Valley, California, USA, 2007–2014, US Geological Survey, 6000 J Street, Placer Hall, Sacramento, CA 95819, USA, doi:10.5194/piahs-372-23-2015

Sözbilir H (2002) Geometry and origin of folding in the Neogene sediments of the Gediz Graben, western Anatolia, Turkey. Geodin Acta 15:277–288

Tonkul, S., Baba, A., Şimşek, C., Durukan, S., Demirkesen, A. C., & Tayfur, G., 2019. Groundwater recharge estimation using HYDRUS 1D model in Alaşehir sub-basin of Gediz Basin in Turkey. *Environmental Monitoring and Assessment*, 191(10), 610.

Ucar, A., & Sariyildiz, S. (2010). An indicator-based assessment for water resources management in Gediz River Basin, Turkey. Water Resources Management, 24(15), 4207-4224.

Winston, R.B., 2022. ModelMuse version 5.0: U.S. Geological Survey Software Release, 18 March 2022, https://doi.org/10.5066/P9JMSQ2M

Xu, CY., Singh, V.P. A Review on Monthly Water Balance Models for Water Resources Investigations. Water Resources Management 12, 20–50 (1998). https://doi.org/10.1023/A:1007916816469

Yercan M., et al., (2004). *Comparative analysis of performance criteria in irrigation schemes: a case study of Gediz river basin in Turkey. , 66(3), 0–266.* doi:10.1016/j.agwat.2003.10.008

Yercan M., Atis E., Salali E.,(2009), Assessing irrigation performance in the Gediz River Basinof Turkey: water user associations versus cooperatives, DOI 10.1007/s00271-008-0142-z

Yi Lixin, et al. ,2011, Land subsidence in Tianjin, China, DOI:10.1007/s12665-010-0604-5

Van Loon, A., Mathijssen, H., & Droogers, P. (2007). Water evaluation and planning system Gediz basin - Turkey. WatManSup report no 5.